



HAL
open science

Highly Emissive Red Heterobimetallic Ir III /M I (M I = Cu I and Au I) Complexes for Efficient Light-Emitting Electrochemical Cells

Anna Bonfiglio, Pei-Wan Hsiao, Yin Chen, Christophe Gourlaouen, Quentin Marchand, Vincent César, Stéphane Bellemin-Laponnaz, Yun-Xin Wang, Chin-Wei Lu, Chantal Daniel, et al.

► **To cite this version:**

Anna Bonfiglio, Pei-Wan Hsiao, Yin Chen, Christophe Gourlaouen, Quentin Marchand, et al.. Highly Emissive Red Heterobimetallic Ir III /M I (M I = Cu I and Au I) Complexes for Efficient Light-Emitting Electrochemical Cells. *Chemistry of Materials*, 2022, 34 (4), pp.1756-1769. 10.1021/acs.chemmater.1c03972 . hal-03789493

HAL Id: hal-03789493

<https://hal.science/hal-03789493>

Submitted on 27 Sep 2022

HAL is a multi-disciplinary open access archive for the deposit and dissemination of scientific research documents, whether they are published or not. The documents may come from teaching and research institutions in France or abroad, or from public or private research centers.

L'archive ouverte pluridisciplinaire **HAL**, est destinée au dépôt et à la diffusion de documents scientifiques de niveau recherche, publiés ou non, émanant des établissements d'enseignement et de recherche français ou étrangers, des laboratoires publics ou privés.

Highly-emissive red heterobimetallic Ir^{III}/M^I (M^I = Cu^I, Au^I) complexes for efficient light-emitting electrochemical cells

*Anna Bonfiglio,¹ Pei-Wan Hsiao,² Yin Chen,² Christophe Gourlaouen,³ Quentin Marchand,⁴
Vincent César,⁴ Stéphane Bellemin-Laponnaz,¹ Yun-Xin Wang,⁵ Chin-Wei Lu,⁵ Chantal
Daniel,³ Federico Polo,⁶ Hai-Ching Su,^{2,*} and Matteo Mauro^{1,*}*

¹ Institut de Physique et Chimie des Matériaux de Strasbourg (IPCMS) UMR7504, Université
de Strasbourg & CNRS, 23 rue du Loess, 67083 Strasbourg (France), e-mail:
mauro@unistra.fr

² Institute of Lighting and Energy Photonics, National Yang Ming Chiao Tung University,
Tainan 71150, Taiwan, e-mail: haichingsu@mail.nctu.edu.tw

³ Laboratoire de Chimie Quantique, Institut de Chimie UMR7177, CNRS-Université de
Strasbourg, 4 Rue Blaise Pascal 67070 Strasbourg (France)

⁴ LCC-CNRS UPR8241, Université de Toulouse, CNRS, 205 route de Narbonne, 31077
Toulouse cedex 4 (France)

⁵ Department of Applied Chemistry, Providence University, Taichung 43301, Taiwan

⁶ Department of Molecular Sciences and Nanosystems, Ca' Foscari University of Venice, Via
Torino 155, 30172 Venezia (Italy)

ABSTRACT

A class of four bright heterobimetallic emitters is presented, which features both a chromophoric $[\text{Ir}(\text{C}^{\wedge}\text{N})_2]$ center and a positively charged, linear *bis*-NHC M(I) ancillary moiety bridged through a Janus-type ligand. In-depth investigation of their optical and electrochemical properties is also reported, which are further elucidated by means of time-dependent density functional theory including spin-orbital coupling effects. All complexes display efficient, vibrant red phosphorescent with higher quantum yield and faster radiative rate constant compared to the parental mononuclear parental complexes. This effect was elucidated in terms of better S-T excited state mixing as well as increased rigidity favored by the multi-metallic architecture. Finally, their electroluminescence performances are investigated by using these bimetallic complexes as electroactive materials in light-emitting electrochemical cells (LECs), achieving external quantum efficiency (EQE) values up to 6% and resulting in amongst the most efficient ones for red emitters. This result is also attributable to the charge-neutral nature of emitting Ir complex bearing a charged, wider energy gap, metal complex as an ancillary moiety.

Introduction

Light-emitting Electrochemical Cells (LECs) are optoelectronic devices in which a single layer of an emissive electroactive material is sandwiched between two electrodes, typically indium tin oxide (ITO) and an air-stable metal, acting as anode and cathode, respectively. LECs are fabricated by solution processing techniques and, therefore, could represent a cheaper and simpler alternative to the more widely explored Organic Light-Emitting Diodes (OLEDs). LECs are particularly attractive for the fabrication of large-area devices for lighting technologies. As for OLED counterparts, in a LEC charge carriers recombine following spin statistics yielding an overall 1:3 singlet-to-triplet exciton ratio. Nevertheless, LEC devices still display lower efficiency and reduced lifetime compared to OLED at comparable spectral region, in spite of the research efforts that have been currently made.^[1-3]

LEC requires the presence of mobile ions that migrate upon application to a suitable electrical bias, ensuring efficient charge injection, migration and recombination within the electroactive layer.^[4-6] For this reason, ionic transition metal complexes (iTMCs) are typically employed acting as both charge-transporting and electroluminescent materials. Compared with neutral TMCs, the main advantage of utilizing iTMCs in LECs is that they are intrinsically charged and no additional electrolyte may be needed in principle. Nevertheless, ionic liquids and/or inorganic salts are often added to speed up the device response of LECs based on iTMCs. In this framework, mononuclear cationic iridium complexes bearing cyclometalated ligands have demonstrated being leading emitting materials,^[7] although sparse examples of anionic derivatives are also known.^[8] This is mainly due to the fact that they are robust compounds possessing relatively high photoluminescence quantum yield (PLQY) and good redox properties, concomitantly, yielding LEC devices with electroluminescence spectra spanning the entire visible spectrum and beyond.^[9-19] Despite, it should be noticed that ionic transition metal

complexes (iTMCs) typically display lower PLQY in comparison with neutral counterparts, which represents a drawback for their efficient applications in light-emitting devices.

One of the issues to address concerning luminescent compound is the severe drop of PLQY when moving towards longer wavelengths, making the design and preparation of compounds that efficiently emit in the red to the near-infrared (NIR) particularly challenging. The origin of this intrinsic limitation has two main causes. On one hand, increase of the vibronic coupling between the potentially-emitting excited state and electronic ground state takes place; a phenomenon described by the so-called *energy gap law*.^[20-23] This coupling provides for efficient radiationless pathways and causes detrimental increase of the non-radiative rate constants (k_{nr}). On the other hand, the radiative rate constant (k_r) scales with the third power of the emission energy, as described by the Einstein quantum theory of radiation. Both effects cause detrimental consequences on the PLQY of red/NIR emitters. Nevertheless, achieving high efficiency in this spectral region is of pivotal importance for device technology given the wide potential application in lighting, telecommunication, encryption, (bio-)sensing and medical care devices.

Bimetallic complexes are rapidly emerging as an attractive alternative to overcome the abovementioned drawbacks.^[24-28] Indeed, suitable design strategies may provide *i*) enhanced spin-orbit coupling (SOC) that induces faster radiative rate constants via increase of SOC constant and/or S–T mixing;^[29–37] and *ii*) more rigid scaffold that helps suppressing radiationless deactivation channels.^[38-39] Therefore, the exploration of novel design strategies for red to NIR emitters is of paramount importance to achieve highly performing electroluminescent devices in this challenging spectral region. Only a very limited number of works describes the application of dinuclear and/or multinuclear complexes in LEC devices and External Quantum Efficiency (EQE) still below 2% have been reported to date.^[33,40-42]

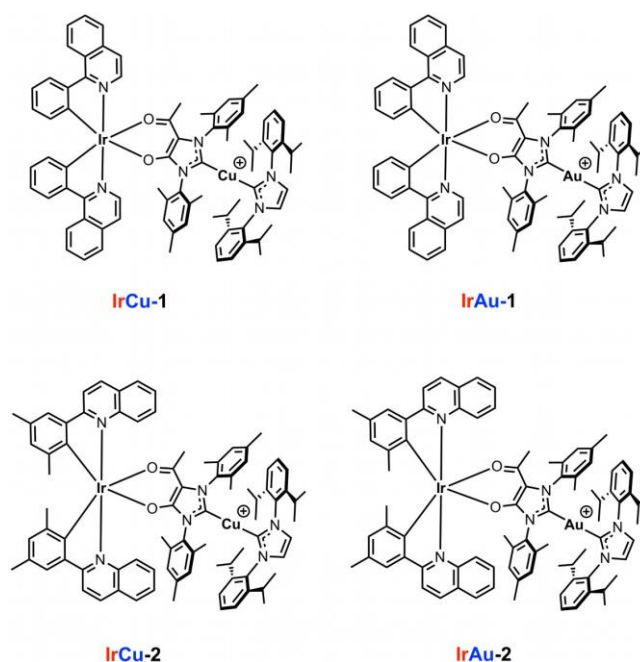
Herein, we describe a series of red highly-emissive cationic hetero-bimetallic complexes for which detailed photophysical, electrochemical, electroluminescence characterization is reported. Furthermore, optical properties were thoroughly elucidated by (time-dependent) density functional theory, namely (TD-)DFT, also including spin-orbit coupling effects. Our proposed design strategy, which consists of neutral iridium-core emitters bearing side-charged moieties, resulted into electroluminescent materials for efficient LECs that remarkably display amongst the highest performances for red triplet emitters in spite of the simple device architecture.

Results and discussion

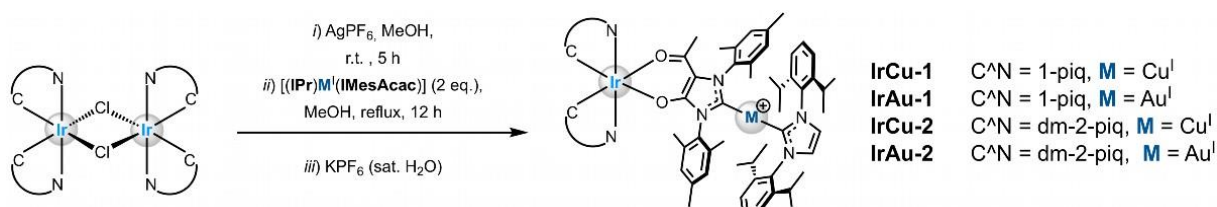
Synthesis

The chemical structure of the four investigated complexes is displayed in Scheme 1, whereas the synthetic pathway employed is shown in Scheme 2 and it is based on previous investigation recently reported by us.^[37] The synthesis starts from the preparation of the chloro-bridged dinuclear complexes of formula $[\text{Ir}(\text{C}^{\wedge}\text{N})_2\text{Cl}]_2$, where $\text{C}^{\wedge}\text{N}$ is either **1-piq** (series 1) or **dm-2-pq** (series 2), where **1-piq** and **dm-2-pq** are 1-phenylisoquinoline and dimethyl-2-phenylquinoline, respectively, by employing the Nonoyama reaction^[43] during which a slight excess of the corresponding $\text{HC}^{\wedge}\text{N}$ proligand is reacted with $\text{IrCl}_3 \cdot n\text{H}_2\text{O}$ in a 3:1 mixture of 2-ethoxyethanol:water. Subsequently, breakage of the dinuclear iridium derivative is achieved by dehalogenation with AgPF_6 salt in MeOH followed by the addition of two equiv. of the metalloproligand $[(\text{IPr})\text{M}^{\text{I}}(\text{IMesAcac})]$ under mild condition, where $\text{M}^{\text{I}} = \text{Cu}^{\text{I}}$ or Au^{I} , $\text{IPr} = 1,3$ -(2,6-diisopropylphenyl)-2*H*-imidazol-2-ylidene and $\text{IMesAcac} = 1,3$ -dimesityl-5-acetylimidazol-2-ylidene-4-olate. Anion metathesis with KPF_6 followed by purification on silica gel plug with CH_2Cl_2 and recrystallization in $\text{CH}_2\text{Cl}_2:\text{Et}_2\text{O}$ provide the target complexes in good to high yield with purity suitable for further photophysical, electrochemical and electroluminescence

characterization. The ^1H , $^{13}\text{C}\{^1\text{H}\}$ NMR as well as high-resolution ESI-MS spectra of the complexes are displayed in Figure S1–S4 of the Supporting Information.



Scheme 1. Chemical structure of the investigated cationic bimetallic complexes **IrCu-1**, **IrAu-1**, **IrCu-2** and **IrAu-2**. All compounds have been prepared as the PF_6^- salt.



Scheme 2. Schematic synthetic pathway followed for the preparation of the target heterobimetallic complexes investigated.

For compounds **IrCu-1** and **IrAu-2**, their atom connectivity was unambiguously ascertained by solving the single-crystal structure with X-ray diffractometric techniques, but the quality of their single crystals was not sufficient to achieve a complete crystallographic resolution.

Nevertheless, basic connectivity was verified (see Figure 1; crystallographic data for complex **IrCu-1** and **IrAu-2** can be found in Table S1 and Table S2 of the Supporting Information, respectively). For both derivatives, the structure confirmed the *trans*-N,N arrangement of the two cyclometalating C[^]N around the iridium(III) atom with a pseudo-octahedral coordination geometry. The coordination sphere of the Ir center is completed by the coordination of the linear *bis*-carbenic [(IPr)M^I(IMesAcac)] complex through the κ^2 :O,O motif (acac moiety). The monovalent M(I) atom is coordinated to the two different NHC ligand forming a linear heteroleptic complex, as expected.

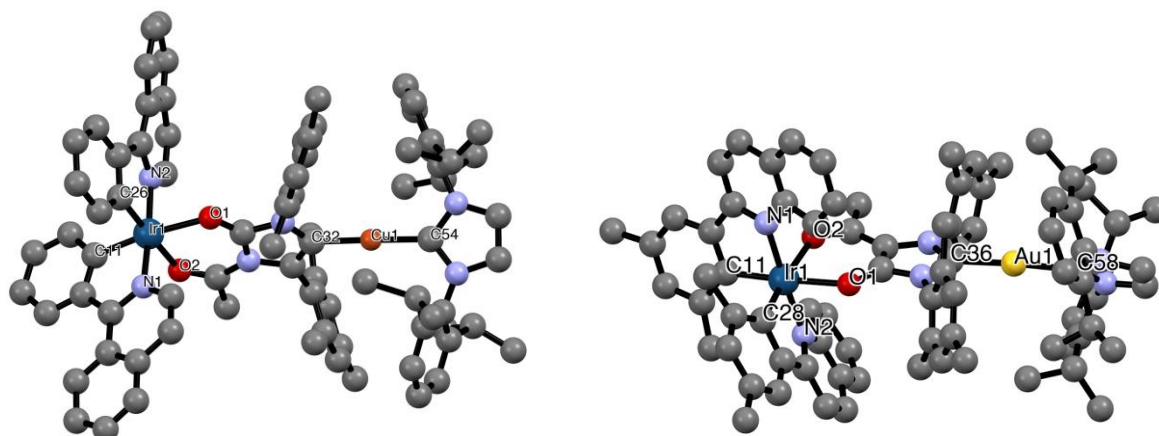


Figure 1. Single-crystal X-ray structure solved for compound **IrCu-1** (left) and **IrAu-2** (right).

Hydrogen atoms and PF_6^- anion are omitted for clarity. Selected bond lengths (\AA) for **IrCu-1**:

$\text{Ir}(1)\text{-C}(11) = 2.005(9)$; $\text{Ir}(1)\text{-N}(1) = 1.985(18)$; $\text{Ir}(1)\text{-C}(26) = 2.015(8)$; $\text{Ir}(1)\text{-N}(2) = 2.037(17)$; $\text{Ir}(1)\text{-O}(2) = 2.167(11)$; $\text{Ir}(1)\text{-O}(1) = 2.182(13)$; $\text{Cu}(1)\text{-C}(32) = 1.92(2)$; $\text{Cu}(1)\text{-C}(54) = 1.921(12)$. For **IrAu-2**: $\text{Ir}(1)\text{-C}(11) = 2.035(10)$; $\text{Ir}(1)\text{-C}(28) = 1.995(11)$; $\text{Ir}(1)\text{-N}(1) = 2.083(9)$; $\text{Ir}(1)\text{-N}(2) = 2.058(8)$; $\text{Ir}(1)\text{-O}(1) = 2.216(6)$; $\text{Ir}(1)\text{-O}(2) = 2.198(7)$; $\text{Au}(1)\text{-C}(36) = 2.023(11)$; $\text{Au}(1)\text{-C}(58) = 2.026(12)$.

Photophysical investigation

The photophysical properties of the four complexes were firstly investigated in CH₂Cl₂ solution at concentration of 3×10⁻⁵ M in both air-equilibrated and degassed condition at room temperature. A list of the most meaningful photophysical data is compiled in Table 1 and the corresponding absorption and photoluminescence spectra at room temperature are displayed in Figure 2. Excitation and low temperature (77 K) emission spectra are displayed in Figure S5 and S6 of the Supporting Information, respectively. For complex **IrCu-1** and **IrAu-1**, photophysical characterization in acetone solution was reported by us previously.^[37] At first glance, UV-vis absorption of the four complexes evidenced similarities in the overall profile of the transitions expectantly, owing to the rather similar electronic properties of the 1-phenyl-isoquinoline and 2-(dimethylphenyl)-quinoline ligands.^[44] Also, within homologous series of complexes bearing the same C^N ligands, a minor role is played by the nature of the M(I) center in the lower energy side of the spectra. In the higher energy region at λ_{abs} = 340–350 nm, all four complexes display intense (ε = 2.06–2.28×10⁴ M⁻¹ cm⁻¹) bands that can be ascribed to electronic processes with mainly singlet-manifold ligand centered (¹LC) to a certain degree of admixing with spin-allowed metal-to-ligand charge transfer (¹MLCT). At lower energy (λ_{abs} *ca.* 400 nm), the less intense transitions with ε = 6.8–8.3×10³ M⁻¹ cm⁻¹ are attributable to electronic processes with mainly ¹MLCT character admixed intraligand charge transfer (¹ILCT). Broader, featureless and much less intense bands can be observed in the region at λ_{abs} *ca.* 470 nm ascribed to a transition with mainly ¹MLCT character with partial ¹LC contribution. The much weaker spectral feature at *ca.* 565 nm is attributed to the ³MLCT transition enabling population of the lowest-lying triplet state through the formally spin-forbidden S₀ → T₁ process. This finding derives from the large SOC effect exerted by the heavy metal atom (Ir) that yields partial relaxation of spin selection rules and enables direct optical excitation of T₁ from the

singlet ground state. All these assignment are based on previously investigations on related derivatives^[45] and are further supported by TD-DFT analysis (*vide infra*).

Upon excitation on the lower-lying bands, dilute CH₂Cl₂ samples of all four the compounds display intense vibrant red emission. In particular, compound **IrCu-1** and **IrAu-1** show a broad emission band centered at $\lambda_{em} = 610$ with a vibrational feature at 645 nm that can be ascribed to an emission originating from an excited state with admixed ³MLCT/³LC character involving the heavy atom and the C^N ligands. On the other hand, emission spectral profile of compound **IrCu-2** and **IrAu-2** are broad, featureless and narrower than those of **IrCu-1** and **IrAu-1**, indicating higher ³MLCT character and lesser geometrical distortion of the emissive excited state for compounds in series 2. Derivatives bearing the dm-2-pq ligand displayed higher PLQY amongst the series, with values as high as 0.77 and 0.73 for the **IrCu-2** and **IrAu-2**, respectively, in degassed CH₂Cl₂. It is worth to notice that these PLQY values are remarkably high and amongst the highest for cationic red-emitting complexes.

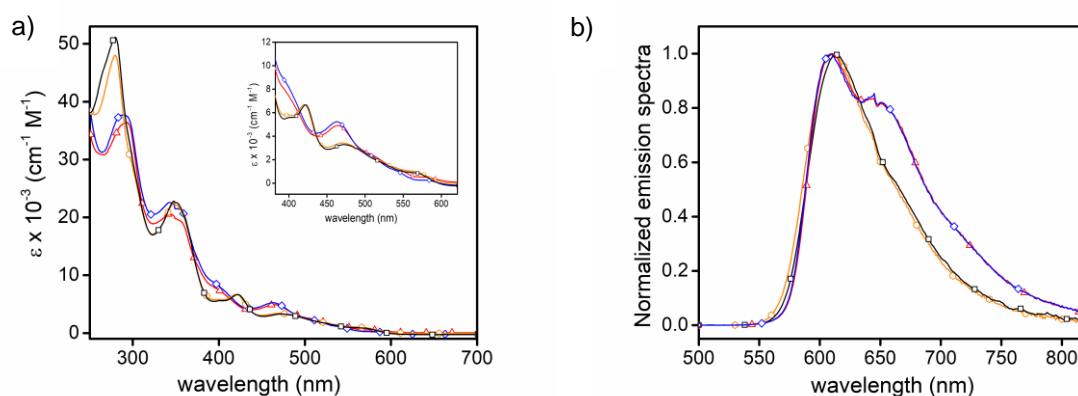


Figure 2. Electronic absorption (a) and emission spectra (b) for **IrCu-1** (red trace), **IrAu-1** (blue trace), **IrCu-2** (black trace) and **IrAu-2** (orange trace) in dichloromethane at concentration of 3.0×10^{-5} M in degassed condition. Samples were excited at $\lambda_{exc} = 420, 460, 480$ and 480 nm for compound **IrCu-1**, **IrAu-1**, **IrCu-2** and **IrAu-2**, respectively. *Inset:* enlarged view of the low-energy side of the absorption spectral profile.

Table 1. Photophysical data recorded for compound **IrCu-1**, **IrAu-1**, **IrCu-2**, **IrAu-2** in degassed CH₂Cl₂ solution at concentration of 3×10⁻⁵ M at room temperature as well as in frozen 2-MeTHF glassy matrix at 77 K. Literature data of the two benchmarks complexes [Ir(1-piq)₂(acac)] and [Ir(dm-2-pq)₂(acac)] are listed as well for sake of comparison.

Compound	λ_{abs} (ϵ) [nm, (10 ³ M ⁻¹ cm ⁻¹)]	λ_{em} ^b [nm]	PLQY ^{b,c} (%)	PLQY ^{b,d} (%)	Lifetime ^{b,c} [ns]	Lifetime ^{b,d} [μ s]	k_{r} [×10 ⁵ s ⁻¹]	k_{nr} [×10 ⁵ s ⁻¹]	λ_{em} ^e [nm]	Lifetime ^e [μ s]
IrCu-1	344 (20.57), 398 (7.57), 463 (4.76), 564 (0.58)	610, 645	8.7	40.5	361	1.6	2.5	3.7	597, 646, 709	2.8
IrAu-1	341 (22.83), 399 (8.30), 464 (5.31), 564 (0.04)	610, 645	9.0	45.5	358	1.7	2.7	3.2	595, 646, 706	2.8
IrCu-2	350 (22.65), 421 (6.76), 470 (3.40), 566 (1.21)	614	7.9	77.0	183	1.8	4.3	1.3	588, 633	7.6
IrAu-2	350 (22.65), 421 (6.76), 470 (3.40), 566 (1.21)	611	8.2	72.8	179	1.8	4.0	1.5	582, 632	7.5
[Ir(1-piq)₂(acac)]^{a)}	-	622	-	0.20	-	1.1	1.8	7.3	-	-
[Ir(dm-2-pq)₂(acac)]^{a)}	-	623	-	0.50	-	1.7	2.9	2.9	-	-

^a Data from Ref. #45. ^b CH₂Cl₂ solution at concentration of 3×10⁻⁵ M at room temperature. ^c Air-equilibrated sample. ^d Degassed sample. ^e Frozen 2-MeTHF glassy matrix at 77 K.

The triplet nature of the radiative process was further corroborated by both the increase of the PLQY and prolongation of the excited state lifetime when going from air-equilibrated to degassed condition. Interestingly, degassed samples of **IrCu-2** and **IrAu-2** show an almost two-fold higher PLQY in comparison with **IrCu-1** and **IrAu-1** despite the rather similar excited-state lifetime. Once again, this result corroborates a larger degree of ³MLCT character for excited state in the series bearing the dm-2-pq ligand. This is also in agreement with the higher extinction coefficient observed for the lowest energy side of the absorption spectrum, attributable to the ³MLCT band,^[45] for **IrCu-2** and **IrAu-2** when compared with **IrCu-1** and **IrAu-1** (see Figure 2a, inset) as well as low temperature measurements (*vide infra*). Further comparison with the photophysical properties of the corresponding mononuclear parental complexes [Ir(1-piq)₂(acac)] and [Ir(dm-2-pq)₂(acac)], where acac is acetylacetonate, provides interesting insights concerning the origin of such remarkably high PLQY values (see Table 1). Overall, the investigated bimetallic species possess smaller k_{nr} values when compared to the monometallic counterparts, indicating that non-radiative channels are suppressed to a larger extent and, therefore, bimetallic structures help providing a more rigid scaffold.

Even more interestingly, k_r values are higher for bimetallic species. In general, the radiative rate of the transition between the T₁ and S₀ can be expressed as follows for a transition metal complex (eqn. 1):^[45, 46]

$$k_r \propto \bar{\nu}^3 \left| \sum_m \frac{\langle S_m | \hat{H}_{SO} | T_1 \rangle}{E_{T_1} - E_{S_m}} \cdot \langle S_0 | er | S_m \rangle \right|^2 \quad \text{eqn. 1}$$

where $\bar{\nu}$ is the electronic transition energy expressed in cm⁻¹, er is the electric dipole operator, the term $\sum_m \frac{\langle S_m | \hat{H}_{SO} | T_1 \rangle}{E_{T_1} - E_{S_m}}$ in the squared brackets relates with the SOC matrix elements between the singlet S_m and the T₁ state, and the matrix element of the second term, $\langle S_0 | er | S_m \rangle$, represents the transition dipole moment of the spin-allowed transition between singlet ground

state S_0 and the higher-lying S_m state, E_{T_1} and E_{S_m} is the energy of the T_1 and S_m state, respectively.

Within each of the two homologous series investigated both absorption and emission features are very similar also in comparison with the mononuclear parental complexes. As such, the terms $\bar{\nu}$ and $\langle S_0 | \mathbf{er} | S_m \rangle$ can be considered being constant. Likewise, SOC matrix elements $\langle S_m | \hat{H}_{SO} | T_1 \rangle$ for involved states are expected to be similar for the four complexes (details on the composition of lower-lying excited states are discussed in the computational investigation and in the Supporting Information, see below and Table S5). Hence, larger k_r values in the bimetallic species are mainly attributed to the smaller energetic gap between the admixing T_1 and S_m states. Hence, the overall enhancement of the PLQY values is attributable to the concomitant increase of k_r and decrease of k_{nr} .

Going from room temperature to frozen in 2-MeTHF glassy matrix at 77 K, all the samples show an emission profile with enhanced vibronic progression and hypsochromically shifted spectra (see Figure 1 and Table 1). In particular, samples of series 1 show a shift of 360–410 cm^{-1} , whereas a much larger shift is observed for compounds of series 2, being as high as 720–810 cm^{-1} .

Moreover, the photophysical properties of thin-film samples prepared by spin-coating techniques were investigated in *poly*-(methyl methacrylate) (PMMA) at 25 wt.% doping level, neat film prepared from CH_2Cl_2 solutions as well as in BMIM[PF₆]:**complex** at 20:80 wt.% ratio in acetonitrile. The corresponding emission spectra are displayed in Figure S7–S9 of the Supporting Information and the photophysical data are summarized in Table 2. In thin-film, emission spectra of all the samples display bathochromic shift compared to dilute solution sample, which is accompanied by a drop of the PLQY in condensed phase, expectantly. It is important to notice that the decrease of the emission efficiency, as well as the bathochromic shift, was less dramatic for compounds of series 2, thus supporting the idea that the presence of

additional methyl groups in the chemical structure of the complexes helps to keep the triplet emitters further apart and therefore mitigating aggregation-caused quenching effects and triplet-triplet annihilation phenomena in condensed phase. This is an important point to address in view of their potential application in solid-state light emitting devices (*vide infra*).

Table 2. Photophysical data recorded for compound **IrCu-1**, **IrAu-1**, **IrCu-2**, **IrAu-2** in thin-films samples under different condition upon excitation at $\lambda_{\text{exc}} = 450$ nm.

Compound	λ_{em} [nm]			PLQY (%)		
	PMMA (25 wt.%)	neat	BMIM[PF ₆]: complex 20:80 wt.%	PMMA (25 wt.%)	neat	BMIM[PF ₆]: complex 20:80 wt.%
IrCu-1	620, 647	622	631,658	1.5	0.5	3.3
IrAu-1	620, 649	620	631, 658	6.0	0.5	4.1
IrCu-2	622	623	620	2	0.9	6.5
IrAu-2	610	623	620	7.5	1	6.6

Electrochemical characterization

The electrochemical behavior of the four bimetallic complexes was assessed by cyclic voltammetry (CV) in acetonitrile (ACN)/0.1 M tetra-*n*-butylammonium perchlorate (TBAP). All the electrochemical data are referenced against ferrocene/ferricenium couple as the internal standard and are reported in Table 3. As shown in Figure 3, in the positive-going scan, all compounds showed a main reversible oxidation process, $O_{1,n}$ (with n denoting the investigated compound), whose standard potential $E_{O_1}^0$ decreased progressively from 0.64 V to 0.45 V following the order **IrCu-1**, **IrAu-1**, **IrAu-2** and **IrCu-2**. Instead, in the negative-going scan, two or three reversible and irreversible reduction processes $R_{i,n}$ (where i denotes the process number and n the investigated compound) occurred in the potential range from -2.00 V to -2.67 V. Voltammetric investigations in the full width potential window are shown in Figure 3,

where indication of the electrochemical HOMO–LUMO band gap is also provided (dashed lines).

Moreover, to better appreciate the redox processes, cyclic voltammeteries for both the positive- and negative-going scans were acquired separately (see $O_{I,n}$ and $R_{I,n}$ processes only in the Figure S10, Supporting Information). It is interesting to note that $O_{I,n}$, which is related to the oxidation of the iridium metal center, formally from Ir(III) to Ir(IV), with involvement of the cyclometalated phenyl ring, has a similar value within the two sets of compounds (series 1 and series 2), as the chelating 1-piq and dm-2-pq provide the metal center a similar electron-donating effect. A similar behavior was already observed for the same compounds lacking the second metal center (Cu or Au).^[37]

In the negative-going scan, processes $R_{I,IrCu-1}$ and $R_{I,IrAu-1}$ are reversible (see Figure S10 in the Supporting Information), although the reversibility is lost when the potential scan is progressively made more negative to reach the respective R_3 before reverting the scan direction. The formal potential where measured and are very similar, $E_{R_{1,IrCu-1}}^0 = -2.02$ V and $E_{R_{1,IrAu-1}}^0 = -2.03$ V, respectively. $R_{I,IrCu-2}$ and $R_{I,IrAu-2}$, instead, showed a weak reversibility (see Figure S10 in the Supporting Information), more likely due to chemical instability of the bimetallic complex, which is further enhanced when the potential is progressively made more negative during the scan. However, the formal potentials for both processes were measured and provided the same value ($E_{R_{1,IrCu-2}}^0 = -2.07$ V and $E_{R_{1,IrAu-2}}^0 = -2.07$ V, respectively), meaning that the reduction process is mainly centered on the cyclometalating ligand (either 1-piq or dm-2-pq) with weak or no involvement of the second metal center. It is worth noting that the ratio between the anodic peak current, $i_{p,a}$, for $O_{I,n}$ and the cathodic peak current, $i_{p,c}$, for $R_{I,n}$ is very close to unity for all the compounds, confirming that the processes are monoelectronic.^[48] Additional characterization and further details concerning the electrochemical processes are provided in the Supplementary Information (see Figure S10-S13 and Table S3).

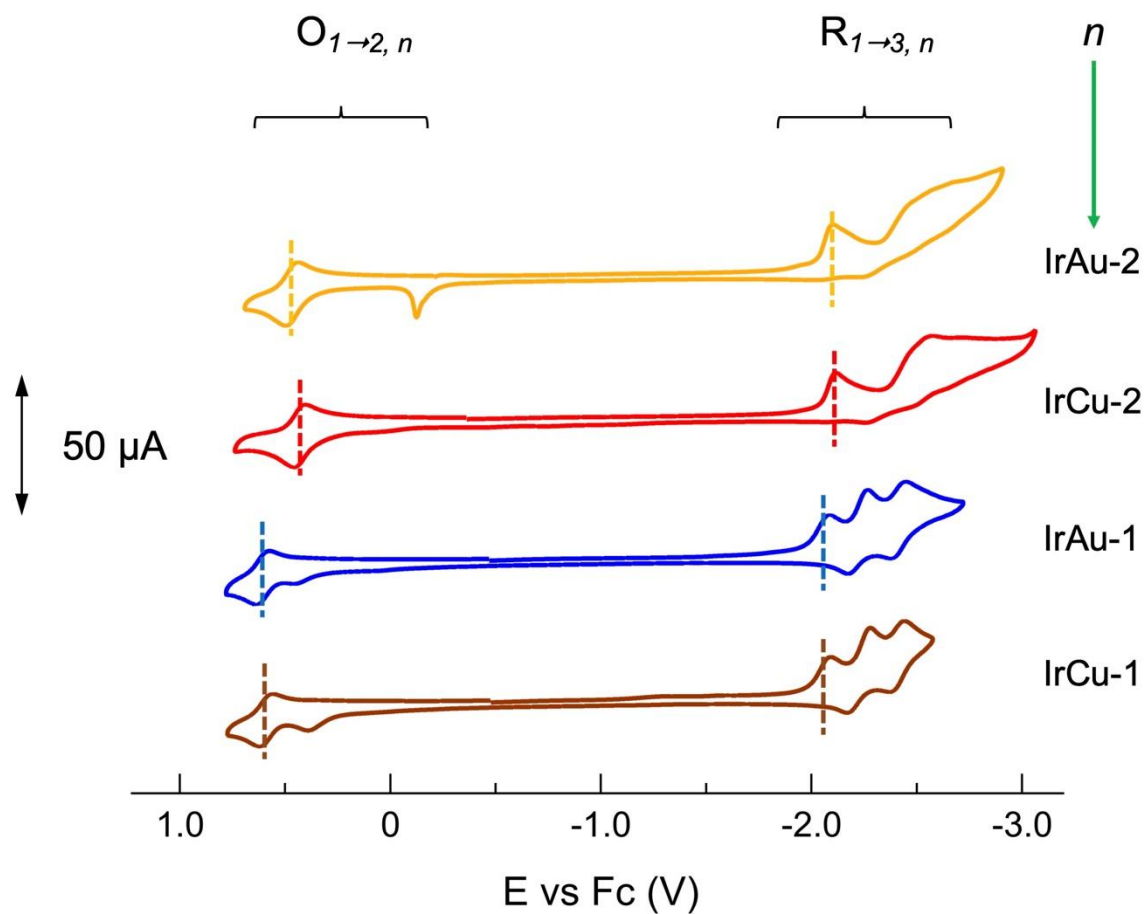


Figure 3. CVs of 1 mM of the investigated compounds in ACN/0.1 M TBAP showing $O_{1-2, n}$ and $R_{1-3, n}$ redox processes. Scan rate: 0.1 V s^{-1} .

Table 3. Electrochemical data for compound **IrCu-1**, **IrAu-1**, **IrCu-2**, **IrAu-2** obtained by cyclic voltammetry (CV) carried out in ACN and 0.1 M TBAP as the supporting electrolyte. All the potential values are referenced to ferrocene/ferricenium couple.

Compound	E^o_{O1} [V] ^a	$\Delta E_{p/2 O1}$ [mV] ^b	E^o_{R1} [V] ^a	$\Delta E_{p/2 R1}$ [mV] ^d	<i>eBand-Gap</i> [eV] ^e
IrCu-1	+0.64	54	-2.02	59	2.66
IrAu-1	+0.62	63	-2.03	63	2.65
IrCu-2	+0.45	60	-2.07	43	2.53
IrAu-2	+0.47	60	-2.07	45	2.54

^a The formal potential is defined as the average value between the cathodic and anodic peak potentials of the investigated redox process, $E_{p,c}$ and $E_{p,a}$, respectively: $E^o = \frac{E_{p,c} + E_{p,a}}{2}$. The values provided are the average values obtained when varying scan rate in the range 0.05-0.5 Vs⁻¹. ^b $\Delta E_{p/2}$ is defined as $E_p - E_{p/2}$, where $E_{p/2}$ is the potential value when the current i is at half its peak value, i_p , for the processes under investigation ($O_{1,n}$ or $R_{1,n}$, respectively). ^c O_2 are irreversible processes. ^d Both R_2 and R_3 processes for **IrCu-1** and **IrAu-1** are reversible, whereas R_2 and R_3 for **IrCu-2** and **IrAu-2** are irreversible, although R_2 for IrCu-2 showed some reversibility for scan rate higher than 0.2 V/s. Therefore, only the peak potential value, E_p , is reported for the latter ones. ^e The eBand-Gap is the electrochemical band-gap between O_1 and R_1 processes.

Theoretical analysis

The structures of the four complexes depicted in Scheme 1 have been fully optimized at the DFT level at their electronic ground state and at the lowest T_1 excited state. The optimized geometries and the associated frontier Kohn-Sham orbitals are depicted in Figure S14 of the Supporting Information. In all complexes both LUMO and LUMO+1 orbitals are localized on the 1-phenyl-isoquinoline (for **IrCu-1** and **IrAu-1**) and 2-methylphenyl-isoquinoline (for **IrCu-2** and **IrAu-2**) ligands. The HOMO involves both the cyclometalated C[^]N ligand and the Ir center, while the HOMO-1 is delocalized over the Ir metal center and the ancillary acac-substituted ligand as exemplified for derivative **IrCu-1** and **IrAu-2** in Figure 4.

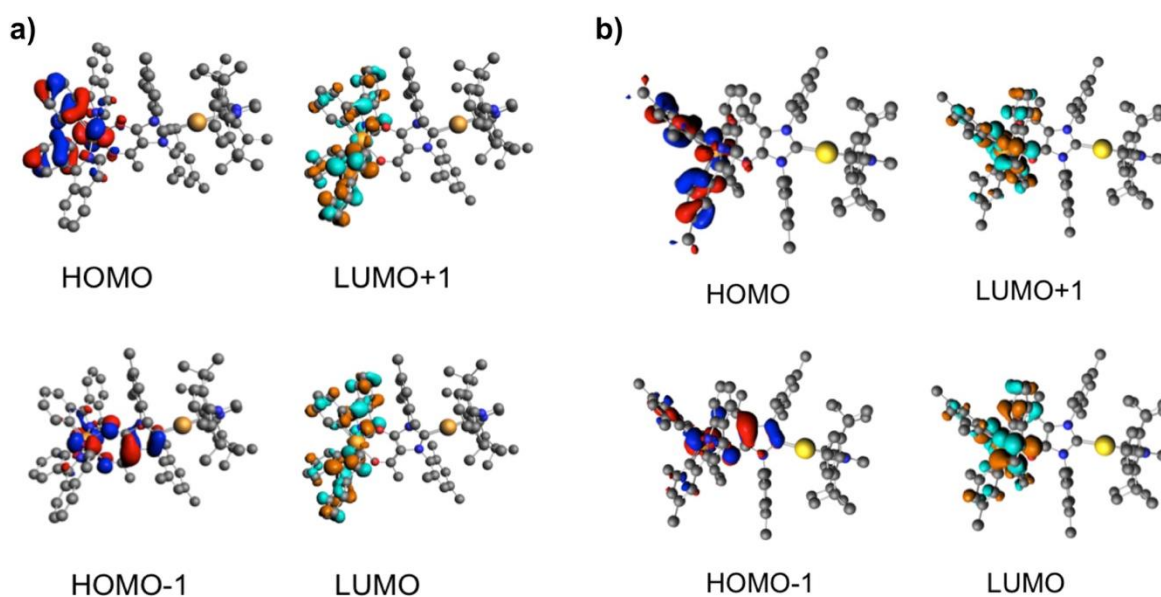


Figure 4. Kohn-Sham frontier orbitals of (a) **IrCu-1** and (b) **IrAu-2**. Hydrogen atoms are hidden for the sake of clarity.

The addition of methyl groups on the phenyl-quinoline ligand modifies the percentage of iridium contribution in the HOMO. Whereas it amounts to 41% in **IrCu-1** and **IrAu-1**, it decreases to 36% in **IrCu-2** and **IrAu-2**. This has consequence on the composition of the low-lying excited states

of mixed LC/MLCT character at Franck-Condon point that characterize the complexes and, consequently, on the extent of SOC on the absorption spectra and photophysical properties. Minor LLCT transitions involving charge transfer between the phenyl-quinoline and the acac ligands contribute to the absorption as illustrated by the electronic density analysis depicted in Figure S15 for **IrCu-1** and **IrAu-2** and in Figure S16 for **IrCu-2** and **IrAu-1** (see Supporting Information section). Computed SOC matrix elements $\langle S_m | \hat{H}_{SO} | T_1 \rangle$ are listed Table S5 of the Supporting Information, highlighting the fact that M^I metal complexes contribute negligibly to the lower-lying excited states. For all complexes, TD-DFT electronic absorption spectra were computed with and without SOC and including solvent effect as well. The spectra are displayed in Figure S17–S19 and detailed discussion on the nature of the transition involved are provided in the Supporting Information.

The contributions of the molecular fragments involved into the charge transfer processes are depicted in Figure S20. As expected, Cu, Au and the NHC ligand (namely, L3) do not significantly contribute to the processes whereas Ir, the phenyl iso-quinoline ligand and to a lesser extent the acac ligands exhibit important contribution to the charge-transfer bands.

At Franck-Condon the LC character of the lowest triplet states is more accentuated as compared to the singlet counterparts. When optimizing the structures of the lowest triplet state the character is modified, T₁ gaining MLCT character as illustrated in Figure 5, where the differences of densities between the electronic ground state and T₁ state are reported and in Figure S21 of the Supporting Information depicting the frontier orbitals of the T₁ states. Whereas the lowest T₁ states of **IrCu-2** and **IrAu-2** possess an ILCT/MLCT character, which corresponds to the HOMO-LUMO transition; the T₁ states of **IrCu-1** and **IrAu-1** features a LC character involving the phenyl-isoquinoline ligand mixed with MLCT as illustrated by the change of electronic densities

depicted in Figure 5. The T_1 states are calculated at 676 nm (**IrCu-1**), 662 nm (**IrCu-2**) and 660 nm (**IrAu-1** and **IrAu-2**).

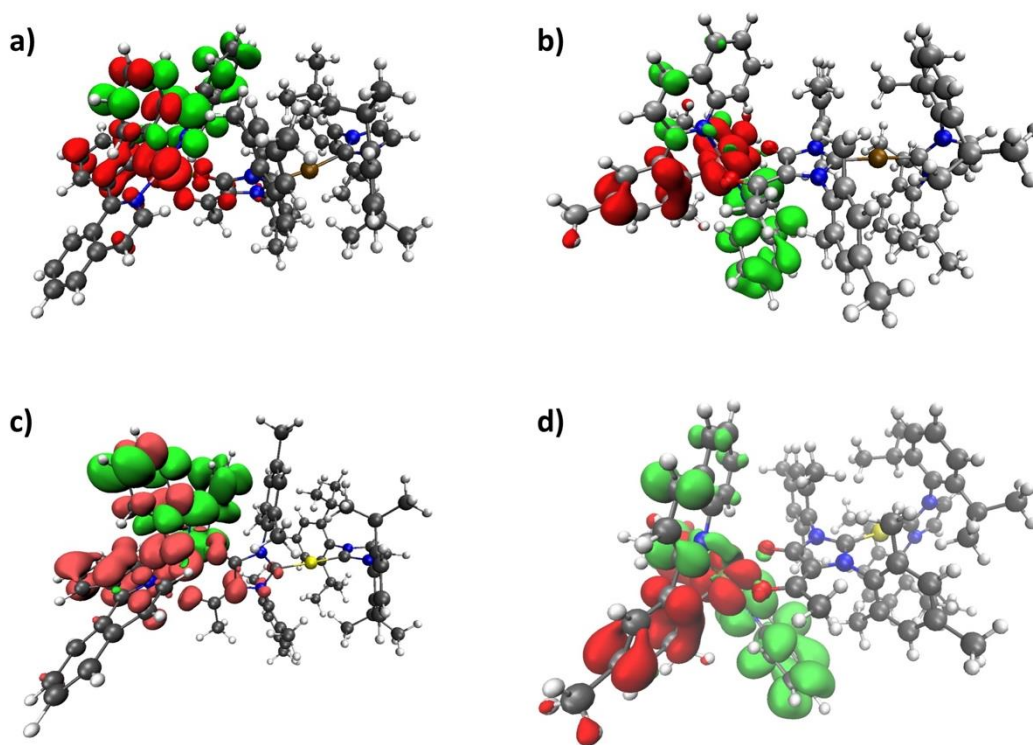


Figure 5. Change of electronic densities when going from the electronic ground state to the lowest T_1 excited state of (a) **IrCu-1**, (b) **IrCu-2**, (c) **IrAu-1** and (d) **IrAu-2**. Loss and gain of density are depicted in red and green color, respectively.

The optimized T_2 states are calculated at about 590 nm for all complexes. Computed value for both T_1 and T_2 state are rather close to the experimental luminescence maximum (see Figure 2 and Table 1), hampering a firm attribution. Indeed, it is important to point out that structure optimization of upper triplet states in this class of large, multi-metallic, molecules is a rather challenging task.

Electroluminescent Characteristics of LECs

To evaluate the EL performance of the proposed heterodinuclear ionic transition metal complexes (iTMCs), the LECs based on complexes **IrCu-1**, **IrAu-1**, **IrCu-2**, and **IrAu-2** were fabricated and their EL characteristics are summarized in Table S6 of the Supplementary Information. All emissive layers of these iTMC were spin-coated from a mixture of the complex (80 wt.%) and [BMIM⁺(PF₆)⁻] (20 wt.%) in acetonitrile solution with various concentrations. Concentration of mixture solution can be tuned to modify the thickness of spin-coated emissive layer. Adjusting emissive layer thickness is an effective approach to optimize light outcoupling efficiency of LECs.^[49-51] The EL spectra of the LECs based on complexes **IrCu-1**, **IrAu-1**, **IrCu-2**, and **IrAu-2** with various emissive-layer thicknesses are depicted in Figure 6. All devices show thickness-dependent EL spectra since altered microcavity effect induced by distinct optical structure and shifted emission zone position modifies wavelength-dependent light in external mode and changes the output EL spectra.^[52-55] Thin-film PL spectra of the emissive layers of LECs based on these complexes are also included in Figure 6 for comparison. In spite of thickness-dependent EL spectra affected by microcavity effect, the EL emissions from the proposed iTMCs are still similar to their PL emissions. Therefore, the proposed iTMCs are excellent candidates for LEC applications.

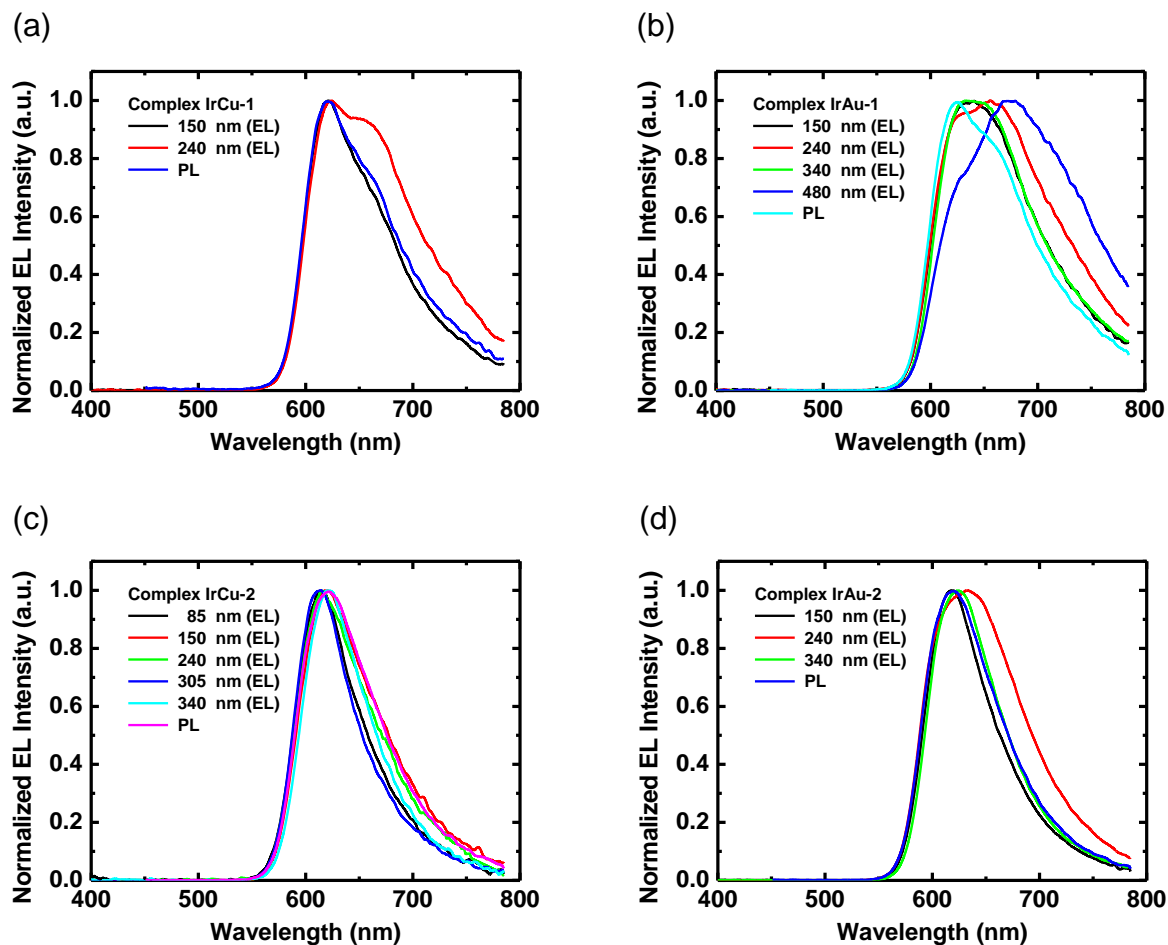


Figure 6. EL spectra of the neat-film LECs based on complexes (a) **IrCu-1**, (b) **IrAu-1**, (c) **IrCu-2**, and (d) **IrAu-2** under 4, 3, 2.5, and 2.5 V, respectively. Thin-film PL spectra of the emissive layers of LECs based on these complexes are also included for comparison.

Time-dependent current densities of the LECs based on complexes **IrCu-1**, **IrAu-1**, **IrCu-2**, and **IrAu-2** are shown in Figure S22a, S23a, S24a, and 7a, respectively. The operating voltages employed in these LECs were kept low and optimized to achieve maximum device efficiencies. Under constant-voltage operation, the time-dependent currents of all LECs show a similar temporal evolution trend. The device current first increases with time after the bias is applied,

reaching a maximum value before decreasing over time. After a bias is applied, the mobile ions in the emissive layer of the LEC are driven toward electrodes and the electrochemically *p*- and *n*-type doped layers are gradually growing. The *p*- and *n*-type doped layers facilitate carrier injection and thus the device current increases with time. When the doped layers are formed completely, the carrier injection rates approach the steady-state regime, and the device current reaches a maximum value. Based on similar emissive-layer thicknesses, *e.g.* 150 or 240 nm, the LECs based on **IrCu-1**, **IrAu-1** exhibit higher device currents than other LECs due to higher bias voltages (*cf.* Figure S22a, S23a, S24a, and 7a). On the other hand, the LECs based on **IrAu-2** (150, 240, or 340 nm) shows higher device currents than the LECs based on **IrCu-2** (150, 240, or 340 nm) under the same bias voltage (*cf.* Figure S24a and 7a). Since complexes **IrCu-2** and **IrAu-2** have similar bandgaps (see Table 3), higher device currents of the LECs based on **IrAu-2** may be attributed to higher carrier mobilities of electroluminescent complex.

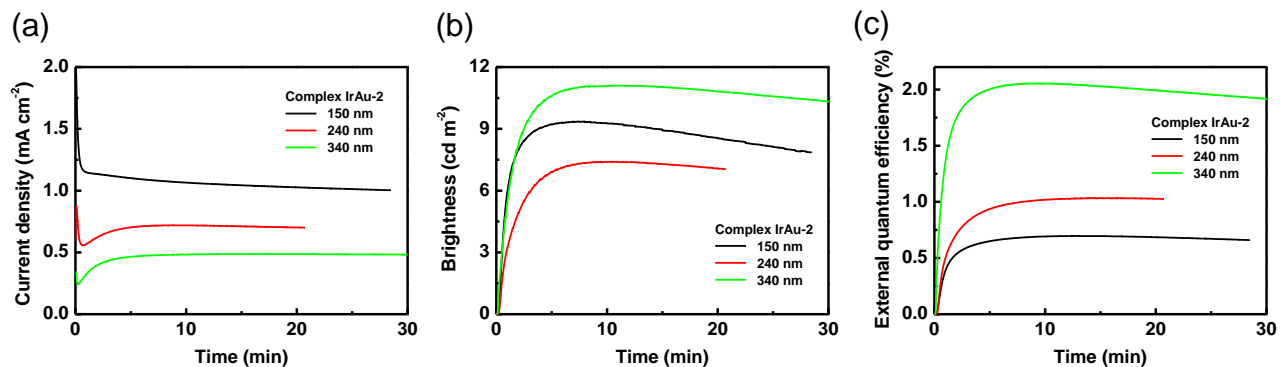


Figure 7. Time-dependent (a) current density, (b) brightness, and (c) EQE of the neat-film LECs based on complex **IrAu-2** under 2.5 V. Thin-film thickness is shown in plot legend.

Time-dependent brightness of the LECs based on complexes **IrCu-1**, **IrAu-1**, **IrCu-2**, and **IrAu-2** are shown in Figure S22b, S23b, S24b, and 7b, respectively. Brightness generally follows the temporal evolution of the device current initially. However, after reaching the maximum value, brightness decreases faster than device current, especially under lower bias voltages. This effect is related to the degradation of emissive material and exciton quenching near the ionic species in the continuously extended doped layers. Under a higher bias voltage, material degradation dominates due to a higher device current and thus decreasing brightness matches well with decreasing device current (*cf.* Figure S22a and S22b). When the bias voltage is reduced, material degradation is mitigated and exciton quenching near doped layers affects brightness reduction more significantly. It is the reason why brightness is decreasing while device current is relatively constant (*cf.* Figure S24a-b, Figure 7a-b).

Time-dependent EQE of the LECs based on complexes **IrCu-1**, **IrAu-1**, **IrCu-2**, and **IrAu-2** are shown in Figure S22c, S23c, S24c, and 7c, respectively. After a bias is applied, the rapid increase in EQE results from improved carrier balance due to the formation of the doped layers. After reaching the peak value, the EQE gradually decreases because of the same reasons responsible for the decrease in brightness with time. The peak EQEs of all LECs improves with increasing emissive-layer thickness (see Table S6). A thicker emissive layer ensures sufficient space between emission zone and doped layers, rendering reduced exciton quenching and improved device efficiency.^[50,56] The LECs based on complexes containing **dm-2-pq** ligand exhibit better EQEs than the LECs based on complexes containing **1-piq** ligands. These results are consistent with higher PLQYs of the thin films of complexes containing **dm-2-pq** ligand blended with 20 wt.% BMIM[PF₆] (Table 2). It can be attributed to the photophysical data revealing a larger degree of ³MLCT character for the excited state of complexes bearing the **dm-2-pq** ligands

(*vide infra*). The optimized LECs based on complex **IrCu-2** and **IrAu-2** show peak EQE as high as 1.73 and 2.05%, respectively. Notably, such device efficiencies are among the highest reported values for the LECs based on multiple-nuclear metal complexes in the literature.^[33,40-42,57-63] It should be pointed out that relatively low device current (brightness) was chosen to obtain better device efficiency. The device efficiency of phosphorescent LECs generally decreases with increasing current due to triplet-triplet annihilation phenomena under a higher triplet exciton density. Increasing the applied bias to 5 V yielded devices with much higher brightness, reaching values as high as 1136 cd cm⁻² when complex **IrAu-2** was employed. Nevertheless, lower EQE values and faster device degradation were observed, expectantly (see Figure S25 of the Supporting Information).

To further increase the device efficiency of LECs, the host-guest strategy has been shown to be effective since the self-quenching effect of the emissive molecules can be reduced.^[17,18,64-67] In this work, relatively more efficient complexes **IrCu-2**, and **IrAu-2** were chosen as guest complexes doped in the host complex **B** (see Figure S26 in the Supporting Information for the chemical structure) to fabricate host-guest LECs. The higher energy gap complex **B**, known to display blue emission, exhibits superior device performance and thus it is suitable for serving as the host complex.^[68] Constant-current mode was employed to optimize the device efficiency of LEC based on complex **B**.^[68] The measured EL properties of the host-guest LECs based on complex **B** doped with complex **IrCu-2** and **IrAu-2** (5 wt.%) are summarized in Table 4 and the EL spectra of the host-guest LECs doped with **IrCu-2** and **IrAu-2** are shown in Figure 8a and 8b, respectively. Compared to the neat-film LECs based on complexes **IrCu-2** and **IrAu-2** (Figure 6c-d), the EL spectra of host-guest LECs possessing distinct optical structure and shifted emission zone position are significantly different due to altered microcavity effect. In addition, different EL

spectra can be observed when adjusting the constant device current. It indicates that the emission zone position moves when the device current changes. In spite of altered EL spectra, the host-guest LECs still exhibit red EL and the color saturation is better than the EL spectra from neat-film LECs.

Table 4. Summary of the device EL characteristics of the host-guest LECs based on emissive layers of host complex **B** doped with guest complex **IrCu-2** or **IrAu-2** (5 wt.%).

Guest complex	Current [μA]	$\lambda_{\text{EL,max}}$ [nm] ^a	B_{max} [cd m ⁻²] ^b	$\eta_{\text{ext,max}}$ (%) ^c	$\eta_{\text{e,max}}$ [cd A ⁻¹] ^d	$\eta_{\text{p,max}}$ [lm W ⁻¹] ^e
IrCu-2	0.1	648	0.25	4.54	2.48	2.54
	0.15	660	0.46	4.23	3.08	3.15
IrAu-2	0.1	641	0.80	6.03	8.05	8.09
	0.15	613	1.53	5.92	10.18	10.16

^a EL peak wavelength of EL spectrum. ^b Maximal brightness. ^c Maximal external quantum efficiency. ^d Maximal current efficiency. ^e Maximal power efficiency.

The time-dependent voltages of the host-guest LECs based on the host complex **B** doped with 5 wt.% guest complexes **IrAu-2** and **IrCu-2** are shown in Figure 9a and Figure S27a of the Supporting Information, respectively. Low operating currents employed in LECs are used to achieve better device efficiency. Under constant-current operation, the time-dependent voltages of both host-guest LECs show a similar decreasing trend. Initially, the electrochemically doped layers are not well formed, and large carrier injection barriers result in higher voltages to reach the required current. During the formation of the electrochemically doped layers, the device voltages decrease rapidly due to significantly reduced carrier injection barriers. Finally, after the

electrochemically doped layers are well formed, the device voltages reach steady states (*ca.* 3.1 V).

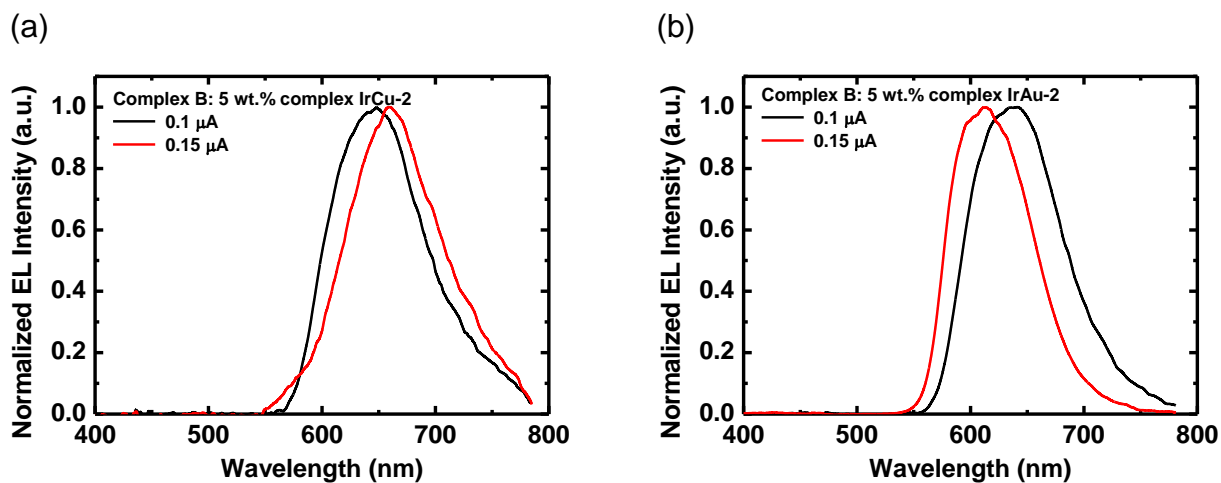


Figure 8. EL spectra of the host-guest LECs based on host complex **B** doped with 5 wt.% guest complex (a) **IrCu-2** and (b) **IrAu-2** under constant currents of 0.1 (black trace) and 0.15 μA (red trace).

The time-dependent brightness and EQEs of the host-guest LECs based on the host complex **B** doped with 5 wt.% guest complexes **IrAu-2** and **IrCu-2** are shown in Figure 9b-c and Figure S27b-c of the Supporting Information, respectively. When the growing electrochemically doped layers reduce the carrier injection barriers gradually, the balance of carrier injection improves and thus the brightness rapidly increases with time under a constant device current. After reaching the maximum brightness, the brightness gradually decreases, which is attributed to emissive material degradation and exciton quenching caused by the extending electrochemically doped layers. Since both host-guest LECs are operated in constant currents, the time-dependent EQE follows a similar trend as the brightness. As expected, both host-guest LECs show significantly enhanced EQEs (>2.6-fold) due to reduced exciton quenching of the guest complex in the host complex **B**. The optimized host-guest LECs based on the host complex **B** doped with 5

wt.% guest complexes **IrCu-2** and **IrAu-2** show the peak EQE of *ca.* 4.5 and 6%, respectively. Such device efficiencies are the highest ever reported for bi and/or multimetallic emitters and amongst the highest for red phosphors, confirming that the proposed heterobimetallic architectures are potential candidates for use in efficient LECs.

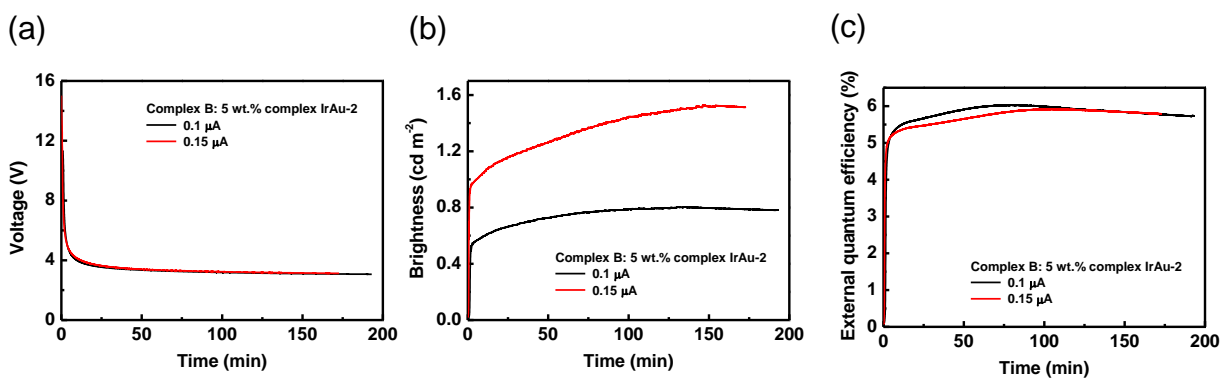


Figure 9. Time-dependent (a) current density, (b) brightness, and (c) EQE of the host-guest LECs based on host complex **B** doped with 5 wt.% guest complex **IrAu-2** under constant currents (0.1 and 0.15 μA).

3. Conclusion

A series of four heterobimetallic emitters is reported that features both a chromophoric [Ir(C^N)₂] center and a positively charged, linear *bis*-NHC M(I) ancillary moiety bridged through a Janus-type ligand. All complexes display efficient, vibrant red phosphorescent with higher quantum yield and faster radiative rate constant compared to the parental mononuclear parental complexes. This effect was elucidated in terms of better S-T excited state mixing as well as increased rigidity favored by the multi-metallic architecture. Involvement of the second metal complex, namely the ancillary [(IPr)M(IMesAcac)], into the lower-lying excited state manifold can be ruled out with confidence as also corroborated by DFT calculations including SOC effects.

The remarkable emission properties of these compounds as well as their suitable redox properties prompted their use as efficient electroactive compounds in solution-processed LECs. Notably, devices based on host-guest architectures with improved charge carrier transport properties displayed outstanding performances reaching the highest EQE values for bi-metallic complexes and amongst the highest for red LECs reported to date. This result is also ascribed to the proposed strategy consisting of a charge-neutral emitting Ir complex bearing a side-charged metal complex with higher-energy gap, resulting in efficient iTMCs. Finally, synthetic efforts employing the presented bi-metallic strategy is currently explored further aiming at compounds with even higher emission PLQY, shorter lifetimes and longer wavelength maxima.

4. Experimental Section

General consideration.

All procedures involving iridium complexes were carried out under an argon atmosphere using standard Schlenk techniques. Nuclear magnetic resonance spectra were recorded using a Bruker Avance III HD 500 MHz spectrometer equipped with a N₂ cryo-probe CPPBBO Prodigy at 298 K. ¹H and ¹³C NMR spectra were calibrated to residual solvent signals.^[69] Elemental analyses were obtained at the AMS Fédération de Chimie Le Bel, University of Strasbourg on a Flash 2000 ThermoFischer Scientific apparatus. HR-ESI-MS spectra were recorded on a MicroToF Bruker equipped with an electrospray ionization source. [(IPr)M^I(IMesAcac)] were synthesized following the procedure reported elsewhere.^[70-71]

Synthesis of the bimetallic complexes. The complexes **IrCu-1**, **IrAu-1**, **IrCu-2** and **IrAu-2** were prepared following the procedure reported by us previously.^[37] [Ir(C[^]N)₂Cl]₂ (1.0 equiv.) was dissolved in 5 mL of methanol and AgPF₆ (2.1 equiv) was added to the mixture. The solution was stirred for 5 hours under argon atmosphere at room temperature. The silver chloride was

filtered off and [(IPr)M^I(IMesAcac)] ligand (2.0 equiv.) was added to the reaction mixture, which was refluxed overnight. After cooling at room temperature, an aqueous solution of KPF₆ was added and a precipitate was formed. The solid was filtered off and washed carefully with water and diethyl ether. A further purification was carried out by chromatographic column on SiO₂, using dichloromethane as eluent. For the collected fractions the volume of the volatiles was reduced under vacuum and diethyl ether was added under stirring to obtain the desired compound as red precipitate.

{[Ir(dm-2-pq)₂][Cu(IPr)](μ-1κ²O,O:2κ¹C-IMesAcac)}PF₆ (IrCu-2): Yield: 75%. ¹H NMR (500 MHz, 298 K, CD₂Cl₂) δ 8.13 (t, *J* = 9.1 Hz, 1H), 7.99 (dd, *J* = 12.3, 8.9 Hz, 1H), 7.75 (d, *J* = 7.9 Hz, 1H), 7.71 (d, *J* = 6.9 Hz, 1H), 7.56 (s, 1H), 7.54–7.44 (m, 2H), 7.41 (t, *J* = 6.2 Hz, 1H), 7.38 – 7.34 (m, 1H), 7.30 – 7.24 (m, 1H), 7.16–7.10 (m, 2H), 7.08–7.03 (m, 1H), 6.98 (s, 1H), 6.70 (d, *J* = 20.5 Hz, 1H), 6.51 (d, *J* = 12.4 Hz, 1H), 6.44 (s, 1H), 2.40 (s, 1H), 2.31 (s, 2H), 2.25 (s, 1H), 2.20 (td, *J* = 13.7, 6.9 Hz, 2H), 1.19 (s, 2H), 1.05 (s, 1H), 1.00 (d, *J* = 6.6 Hz, 6H), 0.80 (s, 1H), 0.74–0.68 (m, 3H), 0.64 (d, *J* = 6.9 Hz, 2H), 0.08 (s, 1H). ¹³C{¹H} NMR (126 MHz, CD₂Cl₂) δ 180.7, 170.0, 169.3, 148.7, 148.3, 148.0, 147.5, 146.4, 146.3, 145.0, 144.7, 141.6, 140.6, 139.3, 138.6, 137.7, 135.1, 135.0, 134.6, 134.4, 134.1, 132.5, 131.2, 131.1, 130.9, 130.4, 130.2, 129.8, 129.7, 129.6, 129.3, 128.1, 127.8, 126.1, 126.0, 126.0, 125.5, 125.0, 124.8, 124.7, 124.6, 124.5, 124.2, 124.1, 123.9, 117.7, 117.3, 29.2, 28.7, 28.5, 28.4, 25.1, 24.1, 24.0, 23.8, 23.5, 23.2, 23.7, 22.3, 21.8, 20.9, 20.6, 18.6, 17.2, 16.6, 15.5, 0.8. HR-ESI-MS: Calcd for [C₈₄H₈₉CuIrN₆O₂]⁺ ([M]⁺): 1469.5967 *m/z*. Found 1469.5969 *m/z*. Anal. Calcd for C₈₄H₈₉CuF₆IrN₆O₂P·2CH₂Cl₂·H₂O: C 57.28 H 5.31 N 4.66. Found: C 56.87 H 5.76 N 5.17.

{[Ir(dm-2-pq)₂][Au(IPr)](μ-1κ²O,O:2κ¹C-IMesAcac)}PF₆ (IrAu-2): Yield: 80%. ¹H NMR (500 MHz, 298 K, CD₂Cl₂) δ 8.14 (dd, *J* = 8.6, 6.0 Hz, 1H), 7.99 (dd, *J* = 15.3, 8.9 Hz, 1H), 7.73

(dd, $J = 16.4, 7.5$ Hz, 1H), 7.57 (s, 1H), 7.54–7.45 (m, 2H), 7.44–7.39 (m, 1H), 7.39–7.35 (m, 1H), 7.29–7.24 (m, 1H), 7.11 (d, $J = 7.8$ Hz, 2H), 7.07–7.03 (m, 1H), 6.70 (d, $J = 10.2$ Hz, 1H), 6.51 (d, $J = 8.2$ Hz, 1H), 6.44 (s, 1H), 2.41 (s, 2H), 2.31 (s, 2H), 2.28–2.14 (m, 3H), 1.43 (s, 1H), 1.30–1.17 (m, 5H), 1.03 (dd, $J = 19.6, 11.1$ Hz, 8H), 0.85 (s, 1H), 0.76 (d, $J = 6.9$ Hz, 2H), 0.71 (d, $J = 6.9$ Hz, 3H), 0.08 (s, 1H). $^{13}\text{C}\{^1\text{H}\}$ NMR (126 MHz, CD_2Cl_2) δ 186.0, 183.0, 181.0, 170.0, 169.3, 157.9, 148.7, 148.3, 148.0, 147.5, 146.3, 146.3, 144.9, 144.9, 141.3, 140.3, 139.3, 138.8, 137.8, 135.0, 134.8, 134.6, 134.5, 133.8, 133.4, 131.3, 131.3, 131.2, 131.2, 131.0, 130.5, 130.3, 129.9, 129.7, 129.6, 129.6, 129.3, 128.2, 127.9, 126.1, 126.1, 126.0, 125.6, 124.8, 124.7, 124.5, 123.9, 117.7, 117.3, 112.3, 28.4, 28.4, 25.3, 23.6, 23.6, 23.4, 23.3, 22.3, 21.8, 21.3, 21.0, 20.6, 20.6, 18.5, 17.1, 16.5, 15.5, 0.8. HR-ESI-MS: Calcd. for $[\text{C}_{84}\text{H}_{89}\text{AuIrN}_6\text{O}_2]^+$ ($[\text{M}]^+$): 1603.6337 m/z . Found: 1603.6437 m/z . Anal. calcd for $\text{C}_{84}\text{H}_{89}\text{AuF}_6\text{IrN}_6\text{O}_2\text{P}\cdot\text{H}_2\text{O}$: C 57.10 H 5.19 N 4.76; found: C 56.87 H 5.17 N 4.70.

Photophysical measurements

Instrument details. Steady-state emission spectra were recorded on a Horiba Jobin–Yvon IBH FL-322 Fluorolog 3 spectrometer equipped with a 450 W xenon arc lamp, double-grating excitation, and emission monochromators (2.1 nm mm^{-1} of dispersion; $1200 \text{ grooves mm}^{-1}$) and a Hamamatsu R13456 red sensitive Peltier-cooled PMT detector. Emission and excitation spectra were corrected for source intensity (lamp and grating) and emission spectral response (detector and grating) by standard correction curves. Time-resolved measurements were performed using either the Time-Correlated Single-Photon Counting (TCSPC) or the Multi-Channel Scaling (MCS) electronics option of the TimeHarp 260 board installed on a PicoQuant FluoTime 300 fluorimeter (PicoQuant GmbH, Germany), equipped with a PDL 820 laser pulse driver. A pulsed laser diode

LDH-P-C-375 ($\lambda = 375$ nm, pulse full width at half maximum <50 ps, repetition rate 200 kHz–40 MHz) was used to excite the sample and mounted directly on the sample chamber at 90° . The photons were collected by a PMA Hybrid-07 single photon counting detector. The data were acquired by using the commercially available software EasyTau II (PicoQuant GmbH, Germany), while data analysis was performed using the built-in software FluoFit (PicoQuant GmbH, Germany).

Luminescence quantum yields were measured in optically dilute solutions (optical density <0.1 at the excitation wavelength) and compared to reference emitter by following the method of Demas and Crosby.^[72–74] The Ru(bpy)₃Cl₂ complex in air-equilibrated water solution at room temperature was used as reference (PLQY = 0.04).^[75] All the solvents were spectrophotometric grade. Deaerated samples were prepared by the freeze–pump–thaw technique by using a home-made quartz cuvette equipped with a Rotaflo stopcock. All the PLQYs on spin-coated thin-film samples were recorded at a fixed excitation wavelength by using a Hamamatsu Photonics absolute PLQY measurements system Quantaury QY equipped with CW Xenon light source (150 W), monochromator, integrating sphere, C7473 photonics multi-channel analyzer and employing the commercially available U6039-05 PLQY measurement software (Hamamatsu Photonics Ltd., Shizuoka, Japan). All measurements were repeated five times at the excitation wavelength $\lambda_{\text{exc}} = 450$ nm, unless otherwise stated.

Methods. For time resolved measurements, data fitting was performed by employing the maximum likelihood estimation (MLE) methods and the quality of the fit was assessed by inspection of the reduced χ^2 function and of the weighted residuals.

Electrochemical setup

Anhydrous acetonitrile (ACN, Sigma-Aldrich, 99.8%) and tetra-*n*-butylammonium perchlorate (TBAP, Fluka, 99%) were used as received. The working electrode was a glassy-carbon disk electrode (2 mm diameter, Princeton Applied Research GO224). The electrode was polished as already described elsewhere.^[76] Before experiments, the electrode was further polished with a 0.05 μm polycrystalline diamond suspension (Buehler, MetaDI) and electrochemically activated in the background solution by means of several voltammetric cycles at 0.5 V s^{-1} between the anodic and the cathodic solvent/electrolyte discharges, until the expected quality features were attained.^[77] A platinum wire served as the counter electrode and a silver wire, separated from the main electrolytic compartment by a Vycor® frit, was used as a quasi-reference electrode. At the end of each experiment, its potential was calibrated against the ferricenium/ferrocene couple, used as an internal redox standard. The cyclic voltammetry (CV) experiments were carried out in ACN/0.1 M TBAP under an Ar atmosphere, using a 1 mM concentration for the electroactive compound. A CHI 760D Electrochemical Workstation (CH Instruments) was used. For the CV experiments, we employed the feedback correction to minimize the ohmic drop between the working and the reference electrodes.

Computational details

The structures of the four complexes in the electronic ground state have been fully optimized at the DFT/B3LYP^[78] level of theory using double- ζ basis sets including scalar relativistic effects for all atoms.^[79] Our previous studies on similar mono- and multimetallic systems^[37] have shown that the use of double- ζ basis sets is justified for the large systems handled here, which could not be handled otherwise. The calculations have been performed in CH_2Cl_2 within the COSMO (conductor-like-screening model) model.^[80] The absorption spectra have been computed at the TD-DFT level (50 roots) including spin-orbit effects at the perturbation level of theory within the

zero-order relativistic approximation (ZORA).^[81–83] The structures of the lowest T₁ triplet states have been optimized at the same level of theory using the Tamm- Dancoff approximation (TDA) in order to avoid triplet instability problems.^[84] The calculations have been performed with the ADF 2019 package (ADF, SCM, Theoretical Chemistry, Vrije Universiteit, Amsterdam, The Netherlands <https://www.scm.com/doc/ADF/index.html>).

LEC Device Fabrication and Characterization

Standard clean and UV/ozone treatments were performed on indium tin oxide (ITO)-coated glass substrates before thin film deposition. Before the emissive layers were deposited, poly(3,4-ethylenedioxythiophene):poly(styrene sulfonate) (PEDOT:PSS) layers (40 nm) were spin-coated at 4000 rpm and then were baked at 150 °C for 30 min in ambient air. The emissive layers of neat-film LECs contained complexes (**IrCu-1**, **IrAu-1**, **IrCu-2** or **IrAu-2**) (80 wt.%) and 1-butyl-3-methylimidazolium hexafluorophosphate [BMIM⁺(PF₆)⁻] (20 wt.%). The ionic liquid [BMIM⁺(PF₆)⁻] was incorporated to provide more mobile ions to speed up the device response. The concentrations of the mixture of the complex and [BMIM⁺(PF₆)⁻] in acetonitrile solutions for complexes **IrCu-1**, **IrAu-1**, **IrCu-2**, and **IrAu-2** were (60 and 100 mg mL⁻¹), (60, 100, 150, and 200 mg mL⁻¹), (30, 60, 100, 120, and 150 mg mL⁻¹), and (60, 100, and 150 mg mL⁻¹), respectively. Spin coating of the mixed acetonitrile solutions was performed at 3000 rpm in ambient air. The thicknesses of spin-coated neat-film emissive layers from mixed acetonitrile solutions of complex **IrCu-1** (60 and 100 mg mL⁻¹), complex **IrAu-1** (60, 100, 150, and 200 mg mL⁻¹), complex **IrCu-2** (30, 60, 100, 120, and 150 mg mL⁻¹), and complex **IrAu-2** (60, 100, and 150 mg mL⁻¹) were (150 and 240 nm), (150, 240, 340, and 480 nm), (85, 150, 240, 305, and 340 nm), and (150, 240, and 340 nm), respectively. For the host-guest LECs, the emissive layers were composed of the

host complex **B**^[85] (75 wt.%), guest complex **IrCu-2** or **IrAu-2** (5 wt.%), and [BMIM⁺(PF₆)⁻] (20 wt.%). The concentration of mixed acetonitrile solution and the thickness of host-guest emissive layer was 200 mg mL⁻¹ and 480 nm, respectively. The thickness of the emissive layer was measured by ellipsometry. The samples were thereafter baked at 70 °C for 10 h in a vacuum oven. Finally, silver top contacts were deposited by thermal evaporation in a vacuum chamber (~10⁻⁶ torr). The EL emission properties of LECs were measured using a source-measurement unit and a calibrated Si photodiode. The EL spectra of these LECs were acquired with a calibrated spectrometer. Neat-film LECs were measured at constant voltages while host-guest LECs were measured at constant currents in a nitrogen glove box to avoid rapid degradation.

SUPPORTING INFORMATION

¹H and ¹³C{¹H} NMR, HR-ESI-MS spectra, additional photophysical, electrochemical and electroluminescence characterization, Cartesian coordinates list of optimized structures and additional theoretical data can be found in the Supporting Information (PDF)

ASSOCIATED CONTENT

CIF files for complex **IrCu-1** and **IrAu-2** (CIF)

AUTHOR INFORMATION

Corresponding Author

* E-mail: mauro@unistra.fr (M.M.)

* E-mail: haichingsu@mail.nctu.edu.tw (H.-C. S.)

Author Contributions

A.B, P.-W.H., Y.C., Q. M., Y.-X. F.P. all contributed to the experimental work. C. G., C.D. performed and analyzed all the computational investigation. M.M. coordinated the work and designed the molecules and photophysical experiments. F.P. performed the electrochemical characterization. H.-C. S. led the device fabrication and the electroluminescence characterization. Q. M., V.C. and S.B.L. contributed to the synthesis of the IMesAcac ligand and metallo-ligands. Y.-X.W. and C.-W.L. synthesized the host complex B. M.M., H.-C. S., F.P., C.G., C.D. analyzed the data and wrote the manuscript. All authors have given approval to the final version of the manuscript.

Notes

The authors declare no competing financial interest.

Funding Sources

The work was financially supported by the Université de Strasbourg, CNRS, The International Centre for Frontier Research in Chemistry (icFRC), and the Labex Chemistry of Complex systems (CSC), the French Agence Nationale de Recherche (ANR), the Institut Carnot MICA, the Higher Education Sprout Project of the National Yang Ming Chiao Tung University and Ministry of Education (MOE, Taiwan).

ACKNOWLEDGMENT

A.B. and M.M. gratefully acknowledge the Université de Strasbourg and CNRS for financial support. The International Centre for Frontier Research in Chemistry (icFRC), and the Labex CSC (ANR-10-LABX-0026 CSC) within the Investissement d'Avenir program ANR-10-IDEX-0002-02 is also acknowledged for funding the PhD fellowship of A.B. M.M. kindly acknowledges the French Agence Nationale de Recherche (ANR) for the grant ANR-18-CE06-007-01. The Institut Carnot MICA is kindly acknowledged for funding the exploratory project "Pt4Poly". This work was supported by the Higher Education Sprout Project of the National Yang Ming Chiao Tung University and Ministry of Education (MOE), Taiwan.

REFERENCES

- [1] *Photoluminescent materials and electroluminescent devices*, Armaroli, N. and Bolink, H. J., Eds.; Springer: Heidelberg, Germany, 2016.
- [2] *Light-emitting Electrochemical Cells: Concepts, Advances and Challenges*, Costa, R. D., Ed. Springer: Heidelberg, Germany, 2017.
- [3] Fresta, E.; Costa, R. D. Beyond traditional light-emitting electrochemical cells – a review of new device designs and emitters. *J. Mater. Chem. C* **2017**, *5*, 5643-5675.
- [4] Pei, Q; Yu, G.; Zhang, C.; Yang, Y.; Heeger A. J. Polymer Light-Emitting Electrochemical Cells. *Science* **1995**, *269*, 1086-1088.
- [5] Pei, Q.; Heeger, A. J. Operating mechanism of light-emitting electrochemical cells. *Nature Mater.* **2008**, *7*, 167-168.
- [6] Slinker, J. D.; DeFranco, J. A.; Jaquith, M. J.; Silveira, W. R.; Zhong, Y.-W.; Moran-Mirabal, J. M.; Craighead, H. G.; Abruña, H. D.; Marohn, J. A.; Malliaras, G. G. Direct

measurement of the electric-field distribution in a light-emitting electrochemical cell. *Nature Mater.* **2007**, *6*, 894-899.

[7] Costa, R. D.; Ortí, E.; Bolink, H. J.; Monti, F.; Accorsi, G.; Armaroli, N. Luminescent Ionic Transition-Metal Complexes for Light-Emitting Electrochemical Cells. *Angew. Chem. Int. Ed.* **2012**, *51*, 8178-8211.

[8] Matteucci, E.; Baschieri, A.; Mazzanti, A.; Sambri, L.; Ávila, J.; Pertegás, A.; Bolink, H. J.; Monti, F.; Leoni, E.; Armaroli, N. Anionic Cyclometalated Iridium(III) Complexes with a Bis-Tetrazolate Ancillary Ligand for Light-Emitting Electrochemical Cells. *Inorg. Chem.* **2017**, *56*, 10584-10595.

[9] Darmawan, N.; Yang, C.-H.; Mauro, M.; Raynal, M.; Heun, S.; Pan, J.; Buchholz, H.; Braunstein, P.; De Cola, L. Efficient Near-UV Emitters Based on Cationic Bis-Pincer Iridium(III) Carbene Complexes. *Inorg. Chem.* **2013**, *52*, 10756-10765.

[10] Yang, C.-H.; Beltran, J.; Lemaur, V.; Cornil, J.; Hartmann, D.; Sarfert, W.; Fröhlich, R.; Bizzarri, C.; De Cola, L. Iridium Metal Complexes Containing N-Heterocyclic Carbene Ligands for Blue-Light-Emitting Electrochemical Cells. *Inorg. Chem.* **2010**, *49*, 9891-9901.

[11] Tordera, D.; Serrano-Pérez, J. J.; Pertegás, A.; Ortí, E.; Bolink, H. J.; Baranoff, E.; Nazeeruddin, Md. K.; Frey, J. Correlating the Lifetime and Fluorine Content of Iridium(III) Emitters in Green Light-Emitting Electrochemical Cells. *Chem. Mater.* **2013**, *25*, 3391-3397.

[12] Bünzli, A. M.; Constable, E. C.; Housecroft, C. E.; Prescimone, A.; Zampese, J. A.; Longo, G.; Gil-Escrig, L.; Pertegás, A.; Ortí, E.; Bolink, H. J. Exceptionally long-lived light-emitting electrochemical cells: multiple intra-cation π -stacking interactions in $[\text{Ir}(\text{C}^{\wedge}\text{N})_2(\text{N}^{\wedge}\text{N})][\text{PF}_6]$ emitters. *Chem. Sci.* **2015**, *6*, 2843-2852.

- [13] Ertl, C. D.; Momblona, C.; Pertegás, A.; Junquera-Hernández, J. M.; La-Placa, M.-G.; Prescimone, A.; Ortí, E.; Housecroft, C. E.; Costable, E. C.; Bolink, H. J. Highly Stable Red-Light-Emitting Electrochemical Cells. *J. Am. Chem. Soc.* **2017**, *139*, 3237-3248.
- [14] Sun, L.; Galan, A.; Ladouceur, S.; Slinker, J. D.; Zysman-Colman, E. High stability light-emitting electrochemical cells from cationic iridium complexes with bulky 5,5' substituents. *J. Mater. Chem.* **2011**, *21*, 18083-18088.
- [15] Henwood, A. F.; Pal, A. K.; Cordes, D. B.; Slawin, A. M. Z.; Rees, T. W.; Momblona, C.; Babaei, A.; Pertegás, A.; Ortí, E.; Bolink, H. J.; Baranoff, E.; Zysman-Colman, E. Blue-emitting cationic iridium(III) complexes featuring pyridylpyrimidine ligands and their use in sky-blue electroluminescent devices. *J. Mater. Chem. C* **2017**, *5*, 9638-9650.
- [16] Su, H.-C.; Chen, H.-F.; Fang, F.-C.; Liu, C.-C.; Wu, C.-C.; Wong, K.-T.; Liu, Y.-H.; Peng, S.-M. Solid-State White Light-Emitting Electrochemical Cells Using Iridium-Based Cationic Transition Metal Complexes. *J. Am. Chem. Soc.* **2008**, *130*, 3413-3419.
- [17] Chen, G.-Y.; Chang, B.-R.; Shih, T.-A.; Lin, C.-H.; Lo, C.-L.; Chen, Y.-Z.; Liu, Y.-X.; Li, Y.-R.; Guo, J.-T.; Lu, C.-W.; Yang, Z.-P.; Su, H.-C. Cationic Ir^{III} Emitters with Near-Infrared Emission Beyond 800 nm and Their Use in Light-Emitting Electrochemical Cells. *Chem. Eur. J.* **2019**, *25*, 5489-5497.
- [18] Yu, G.-X.; Lin, C.-H.; Liu, Y.-X.; Yi, R.-H.; Chen, G.-Y.; Lu, C.-W. Su, H.-C. Efficient and Saturated Red Light-Emitting Electrochemical Cells Based on Cationic Iridium(III) Complexes with EQE up to 9.4%. *Chem. Eur. J.* **2019**, *25*, 13748-13758.
- [19] Su, H.-C.; Chen, Y.R.; Wong, K.-T. Recent Progress in White Light-Emitting Electrochemical Cells. *Adv. Funct. Mater.* **2020**, *30*, 1906898.

- [20] Englman, R. and Jortner, J. The energy gap law for radiationless transitions in large molecules. *Mol. Phys.* **1970**, *18*, 145-164.
- [21] Caspar, J. V. and Meyer, T. J. Photochemistry of MLCT excited states. Effect of nonchromophoric ligand variations on photophysical properties in the series *cis*-Ru(bpy)₂L₂²⁺. *Inorg. Chem.* **1983**, *22*, 2444-2453.
- [22] Caspar, J. V. and Meyer, T. J. Application of the energy gap law to nonradiative, excited-state decay. *J. Phys. Chem.* **1983**, *87*, 952-957.
- [23] Kober, E. M. ; Caspar, J. V.; Lumpkin R. S.; Meyer, T. J. Application of the energy gap law to excited-state decay of osmium(II)-polypyridine complexes: calculation of relative nonradiative decay rates from emission spectral profiles. *J. Phys. Chem.* **1986**, *90*, 3722-3734.
- [24] Puttock, E. V.; Walden M. T.; Williams, J. A. G. The luminescence properties of multinuclear platinum complexes. *Coord. Chem. Rev.* **2018**, *367*, 127-162.
- [25] Zhang, Q.-C.; Xiao, H.; Zhang, Z.; Xu, L.-J.; Chen, Z.-N. Luminescent oligonuclear metal complexes and the use in organic light-emitting diodes. *Coord. Chem. Rev.* **2019**, *378*, 121-133.
- [26] Li, G.; Zhu, D.; Wang, Z.; Su Z.; Bryce, M. R. Dinuclear metal complexes: multifunctional properties and applications. *Chem. Soc. Rev.* **2020**, *49*, 765-838.
- [27] Li, G.; Congrave, D. G.; Zhu, D.; Su Z.; Bryce, M. R. Recent advances in luminescent dinuclear iridium(III) complexes and their application in organic electroluminescent devices. *Polyhedron* **2018**, *140*, 146-157.
- [28] Mauro, M. Phosphorescent multinuclear complexes for optoelectronics: tuning of the excited-state dynamics. *Chem. Comm.* **2021**, *57*, 5857-5870.

- [29] Shafikov, M. Z.; Zaytsev A. V.; Kozhevnikov, V. N. Halide-Enhanced Spin–Orbit Coupling and the Phosphorescence Rate in Ir(III) Complexes. *Inorg. Chem.*, **2021**, *60*, 642-650.
- [30] Shafikov, M. Z.; Daniels R.; Kozhevnikov, V. N. Unusually Fast Phosphorescence from Ir(III) Complexes via Dinuclear Molecular Design. *J. Phys. Chem. Lett.* **2019**, *10*, 7015-7024.
- [31] Yang, X.; Feng, Z.; Zhao, J.; Dang, J.-S.; Liu, B.; Zhang K.; Zhou, G. Pyrimidine-Based Mononuclear and Dinuclear Iridium(III) Complexes for High Performance Organic Light-Emitting Diodes. *ACS Appl. Mater. Interfaces*, **2016**, *8*, 33874-33887.
- [32] Daniels, R. E.; Culham, S.; Hunter, M.; Durrant, M. C.; Probert, M. R.; Clegg, W.; Williams, J. A. G.; Kozhevnikov, V. N. When two are better than one: bright phosphorescence from non-stereogenic dinuclear iridium(III) complexes. *Dalton Trans.*, **2016**, *45*, 6949-6962.
- [33] Shafikov, M. Z.; Tang, S.; Larsen, C.; Bodensteiner, M.; Kozhevnikov, V. N.; Edman, L. An efficient heterodinuclear Ir(III)/Pt(II) complex: synthesis, photophysics and application in light-emitting electrochemical cells. *J. Mater. Chem. C*, **2019**, *7*, 10672-10862.
- [34] Shafikov, M. Z.; Pander, P.; Zaytsev, A. V.; Daniels, R.; Martinscroft, R.; Dias, F. B.; Williams, J. A. G.; Kozhevnikov, V. N. Extended ligand conjugation and dinuclearity as a route to efficient platinum-based near-infrared (NIR) triplet emitters and solution-processed NIR-OLEDs. *J. Mater. Chem. C*, **2021**, *9*, 127-135.
- [35] Hao, Z.; Zhang, K.; Chen, K.; Wang, P.; Lu, Z.; Zhu, W.; Liu, Y. More efficient spin–orbit coupling: adjusting the ligand field strength to the second metal ion in asymmetric binuclear platinum(II) configurations. *Dalton Trans.*, **2020**, *49*, 8722-8733.
- [36] Shafikov, M. Z.; Daniels, R.; Pander, P.; Dias, F. B.; Williams, J. A. G.; Kozhevnikov, V. N. Dinuclear Design of a Pt(II) Complex Affording Highly Efficient Red Emission:

Photophysical Properties and Application in Solution-Processible OLEDs. *ACS Appl. Mater. Interfaces*, **2019**, *11*, 8182-8193.

[37] Bonfiglio, A.; Pallova, L.; César, V.; Gourlaouen, C.; Bellemin-Laponnaz, S.; Daniel, C.; Polo, F.; Mauro, M. Phosphorescent Cationic Heterodinuclear Ir^{III}/M^I Complexes (M = Cu^I, Au^I) with a Hybrid Janus-Type N-Heterocyclic Carbene Bridge. *Chem. – Eur. J.*, **2020**, *26*, 11751-11766.

[38] Zheng, Y.; Batsanov, A. S.; Fox, M. A.; Al-Attar, H. A.; Abdullah, K.; Jankus, V.; Bryce, M. R.; Monkman, A. P. Bimetallic cyclometalated iridium(III) diastereomers with non-innocent bridging ligands for high-efficiency phosphorescent OLEDs. *Angew. Chem., Int. Ed.*, **2014**, *53*, 11616-11619.

[39] M'hamedi, A.; Fox, M. A.; Batsanov, A. S.; Al-Attar, H. A.; Monkman, A. P.; Bryce, M. R. Bright green PhOLEDs using cyclometalated diiridium(III) complexes with bridging oxamidato ligands as phosphorescent dopants. *J. Mater. Chem. C*, **2017**, *5*, 6777-6789.

[40] Costa, R. D.; Fernandez, G.; Sanchez, L.; Martin, N.; Ortí, E.; Bolink, H. J. Dumbbell-Shaped Dinuclear Iridium Complexes and Their Application to Light-Emitting Electrochemical Cells. *Chem. Eur. J.*, **2010**, *16*, 9855-9866.

[41] Fernández-Cestau, J.; Giménez, N.; Lalinde, E.; Montañó, P.; Moreno, M. T.; Sánchez, S.; Weber, M. D.; Costa, R. D. Alkynyl bridged cyclometalated Ir₂M₂clusters: impact of the heterometal in the photo- and electro-luminescence properties. *Dalton Trans.*, **2016**, *45*, 3251-3255.

[42] La-Placa, M.-G.; Igual-Munõz, A. M.; Romero, J.; Daniels, R. E.; Kozhevnikov, V. N.; Sessolo, M.; Bolink, H. J. Red Light-Emitting Electrochemical Cells Employing Pyridazine-Bridged Cationic Diiridium Complexes. *ECS Solid State Sci. Tech.*, **2019**, *8*, R84-R87.

- [43] Nonoyama, M. Benzo[*h*]quinolin-10-yl-N iridium (III) complexes. *Bull. Chem. Soc. Jpn.* **1974**, *47*, 767-768.
- [44] The photophysical properties of compound **IrCu-1** and **IrAu-1** were reported previously in acetone. For sake of comparison, there were re-measured in CH₂Cl₂.
- [45] Yersin, H.; Rausch, A. F.; Czerwieniec, R.; Hofbeck, T.; Fischer, T. The triplet state of organo-transition metal compounds. Triplet harvesting and singlet harvesting for efficient OLEDs. *Coord. Chem. Rev.* **2011**, *255*, 2622-2652.
- [46] *Modern Molecular Photochemistry of Organic Molecules*, Turro, N. J.; Ramamurthy, V.; Scaiano, J. C., Eds.; University Science Books, **2010**.
- [47] Ai, P.; Mauro, M.; Gourlaouen, C.; Carrara, S.; De Cola, L.; Tobon, Y.; Giovanella, U.; Botta, C.; Danopoulos, A. A.; Braunstein, P. Bonding, Luminescence, Metallophilicity in Linear Au₃ and Au₂Ag Chains Stabilized by Rigid Diphosphanil NHC Ligands. *Inorg. Chem.*, **2016**, *55*, 8527-8542.
- [48] *Electrochemical Methods: Fundamentals and Applications*, 2nd Ed., Bard, A. J. and Faulkner, L. R. (Eds) Wiley, **2000**.
- [49] Yi, R.-H.; Lo, C.-L.; Luo, D.; Lin, C.-H.; Weng, S.-W.; Lu, C.-W.; Liu, S.-W.; Chang, C.-H.; Su, H.-C. Combinational Approach To Realize Highly Efficient Light-Emitting Electrochemical Cells. *ACS Appl. Mater. Interfaces* **2020**, *12*, 14254-14264.
- [50] Jhang, Y.-P.; Chen, H.-F.; Wu, H.-B.; Yeh, Y.-S.; Su, H.-C.; Wong, K.-T. Improving device efficiencies of solid-state white light-emitting electrochemical cells by adjusting the emissive-layer thickness. *Org. Electron.* **2013**, *14*, 2424-2430.
- [51] Li, X.; Gao, J.; Liu, G. Thickness dependent device characteristics of sandwich polymer light-emitting electrochemical cell. *Org. Electron.* **2013**, *14*, 1441-1446.

- [52] Lin, G.-R.; Chen, H.-F.; Shih, H.-C.; Hsu, J.-H.; Chang, Y.; Chiu, C.-H.; Cheng, C.-Y.; Yeh, Y.-S.; Su, H.-C.; Wong, K.-T. Non-doped solid-state white light-emitting electrochemical cells employing the microcavity effect. *Phys. Chem. Chem. Phys.* **2015**, *17*, 6956-6962.
- [53] Hsu, J.-H.; Su, H.-C. Host-only solid-state near-infrared light-emitting electrochemical cells based on interferometric spectral tailoring. *Phys. Chem. Chem. Phys.* **2016**, *18*, 5034-5039.
- [54] Su, H.-C. Optical Techniques for Light-Emitting Electrochemical Cells. *ChemPlusChem* **2018**, *83*, 197-210.
- [55] Yang, Z.-P.; Su, H.-C. Recent Advances in Optical Engineering of Light-Emitting Electrochemical Cells. *Adv. Funct. Mater.* **2020**, *30*, 1906788.
- [56] Lee, C.-L.; Cheng, C.-Y.; Su, H.-C. Enhancing device efficiencies of solid-state near-infrared light-emitting electrochemical cells by employing a tandem device structure. *Org. Electron.* **2014**, *15*, 711-720.
- [57] Jia, W.-L.; Hu, Y.-F.; Gao, J.; Wang, S. Linear and star-shaped polynuclear Ru(ii) complexes of 2-(2'-pyridyl)benzimidazolyl derivatives: syntheses, photophysical properties and red light-emitting devices. *Dalton Trans.* **2006**, *35*, 1721-1728.
- [58] Xun, S.; Zhang, J.; Li, X.; Ma, D.; Wang, Z. Y. Synthesis and near-infrared luminescent properties of some ruthenium complexes. *Synth. Met.* **2008**, *158*, 484-488.
- [59] Ju, C.-C.; Chen, C.-H.; Yuan, C.-L.; Wang, K.-Z. Electroluminescence from single-layer thin-film devices based on three binuclear Ru(II) complexes with different length of flexible bridges. *Thin Solid Films* **2011**, *519*, 3883-3889.
- [60] Bizzarri, C.; Strabler, C.; Prock, J.; Trettenbrein, B.; Ruggenthaler, M.; Yang, C.-H.; Polo, F.; Iordache, A.; Brüggeller, P.; De Cola, L. Luminescent Dinuclear Cu(I) Complexes Containing Rigid Tetrphosphine Ligands. *Inorg. Chem.* **2014**, *53*, 10944-10951.

- [61] Bideh, B. N.; Shahroosvand, H. Efficient near infrared light emitting electrochemical cell (NIR-LEEC) based on new binuclear ruthenium phenanthroimidazole exhibiting desired charge carrier dynamics. *Sci. Rep.* **2017**, *7*, 15739.
- [62] Cinninger, L. M.; Bastatas, L. D.; Shen, Y.; Holiday, B. J.; Slinker, J. D. Luminescent properties of a 3,5-diphenylpyrazole bridged Pt(II) dimer. *Dalton Trans.* **2019**, *48*, 9684-9691.
- [63] Shiu, L.-C.; Chang, B.-R.; Hsiao, M. C.-S.; Sie, W.-S.; Wu, M.-L.; Huang, L.-X.; Wang, C.-M.; Lee, G.-H.; Chang, I.-J.; Su, H.-C.; Shiu, K.-B. Alkyl-Spacer Enhancement in Performance of Light-Emitting Electrochemical Cells. *Eur. J. Inorg. Chem.* **2020**, 3517-3526.
- [64] Hosseini, A. R. ; Koh, C. Y.; Slinker, J. D.; Flores-Torres, S.; Abruña, H. D.; Malliaras, G. G. Addition of a Phosphorescent Dopant in Electroluminescent Devices from Ionic Transition Metal Complexes. *Chem. Mater.* **2005**, *17*, 6114-6116.
- [65] Chen, B. ; Li, Y.; Chu, Y.; Zheng, A.; Feng, J.; Liu, Z.; Wu, H. ; Yang, W. Highly efficient single-layer organic light-emitting devices using cationic iridium complex as host. *Org. Electron.* **2013**, *14*, 744-753.
- [66] Pertegás, A.; Shavaleev, N. M.; Tordera, D.; Ortí, E.; Nazeeruddin, M. K.; Bolink, H. J. Host-guest blue light-emitting electrochemical cells. *J. Mater. Chem. C* **2014**, *2*, 1605-1611.
- [67] Moore, M. D.; Bowler, M. H.; Reynolds, J. E.; Lynch, V. M.; Shen, Y.; Slinker, J. D.; Sessler, J. L. Ionic Organic Small Molecules as Hosts for Light-Emitting Electrochemical Cells. *ACS Appl. Mater. Interfaces* **2018**, *10*, 24699-24707.
- [68] Chen, Y.-Z.; Luo, D.; Hsiang, C.-H.; Yi, R.-H.; Lin, C.-H.; Lu, C.-W.; Liu, S.-W.; Chang, C.-H.; Su, H.-C. Highly efficient blue and white light-emitting electrochemical cells employing substrates containing embedded diffusive layers. *Org. Electron.* **2020**, *77*, 105515.

- [69] Fulmer, G. R.; Miller, A. J. M.; Sherden, N. H.; Gottlieb, H. E.; Nudelman, A.; Stoltz, B. M.; Bercaw, J. E.; Goldberg, K. I. NMR Chemical Shifts of Trace Impurities: Common Laboratory Solvents, Organics, and Gases in Deuterated Solvents Relevant to the Organometallic Chemist. *Organometallics* **2010**, *29*, 2176-2179.
- [70] César, V.; Mallardo, V.; Nano, A.; Dahm, G.; Lugan, N.; Lavigne, G.; Bellemin-Laponnaz, S. IMes-acac: hybrid combination of diaminocarbene and acetylacetonato sub-units into a new anionic ambidentate NHC ligand. *Chem. Comm.* **2015**, *51*, 5271-5274.
- [71] César, V.; Mallardo, V.; Nano, A.; DePeter, S. F.; Bastin, S.; Sournia-Saquet, A.; Maise-François, A.; Lugan, N.; Bellemin-Laponnaz, S. Homo- and Heteropolymetallic Complexes of the Hybrid, Ambidentate N-Heterocyclic Carbene Ligand IMes-acac. *ACS Omega* **2018**, *3*, 15582-15591.
- [72] Crosby, G. A. and Demas, J. N. C. Quantum efficiencies of transition-metal complexes. I. d-d Luminescence. *J. Am. Chem. Soc.*, **1970**, *92*, 7262-7270.
- [73] Ishida, H.; Bünzli J.-C.; Beeby, A. Guidelines for measurement of luminescence spectra and quantum yields of inorganic and organometallic compounds in solution and solid state (IUPAC Technical Report). *Pure Appl. Chem.*, **2016**, *88*, 701-711.
- [74] Würth, C.; Grabolle, M.; Pauli, J.; Spieles, M.; Resch-Genger, U. Relative and absolute determination of fluorescence quantum yields of transparent samples. *Nat. Protoc.*, **2013**, *8*, 1535-1550.
- [75] Ishida, I.; Tobita, S.; Hasegawa, Y.; Katoh, R.; Nozaki, K. Recent Advances in Instrumentation for Absolute Emission Quantum Yield Measurements. *Coord. Chem. Rev.*, **2010**, *254*, 2449-2458.

- [76] Antonello, S.; Musumeci, M.; Wayner, D. D. M.; Maran, F. Electroreduction of Dialkyl Peroxides. Activation–Driving Force Relationships and Bond Dissociation Free Energies. *J. Am. Chem. Soc.*, **1997**, *119*, 9541-9549.
- [77] Meneses, A. B.; Antonello, S.; Arévalo, M. C.; Maran, F. Double-Layer Correction for Electron-Transfer Kinetics at Glassy Carbon and Mercury Electrodes in *N,N*-Dimethylformamide. *Electroanalysis*, **2006**, *18*, 363-370.
- [78] Stephens, P. J.; Devlin, F. J.; Chabalowski, C. F.; Frisch, M. J. Ab Initio Calculation of Vibrational Absorption and Circular Dichroism Spectra Using Density Functional Force Fields. *J. Phys. Chem.* **1994**, *98*, 11623-11627.
- [79] Van Lenthe, E.; Baerends, E. J. Optimized Slater-type basis sets for the elements 1–118. *J. Comput. Chem.* **2002**, *24*, 1142-1156.
- [80] Klamt, A. Conductor-like Screening Model for Real Solvents: A New Approach to the Quantitative Calculation of Solvation Phenomena. *J. Phys. Chem.* **1995**, *99*, 2224-2235.
- [81] van Lenthe, E. ; van Leeuwen, R. ; Baerends, E. J.; Snijders, J. G. Relativistic regular two-component Hamiltonians. *Int. J. Quant. Chem.* **1996**, *57*, 281-293.
- [82] Wang, F.; Ziegler, T. A simplified relativistic time-dependent density-functional theory formalism for the calculations of excitation energies including spin-orbit coupling effect. *J. Chem. Phys.* **2005**, *123*, 154102-154112.
- [83] Wang, F.; Ziegler, T.; van Lenthe, E.; van Gisbergen, S. ; Baerends, E. J. The calculation of excitation energies based on the relativistic two-component zeroth-order regular approximation and time-dependent density-functional with full use of symmetry. *J. Chem. Phys.* **2005**, *122*, 204103-204112.

[84] Peach, M. J. G.; Tozer, D. J. Overcoming Low Orbital Overlap and Triplet Instability Problems in TDDFT. *J. Phys. Chem. A* **2012**, *116*, 9783-9789.

[85] Wu, M.-L.; Chen, G.-Y.; Shih, T.-A.; Lu, C.-W.; Su, H.-C. Effects of tuning the applied voltage pulse periods on the electroluminescence spectra of host–guest white light-emitting electrochemical cells. *Phys. Chem. Chem. Phys.* **2018**, *20*, 18226-18232.

TABLE OF CONTENT GRAPHICS

